August 23, 2017

Re: Response to the Comments of Prof. H. Class on Manuscript HESSD-2017--90 (Moment-based Metrics for Global Sensitivity Analysis of Hydrological Systems by A. Dell'Oca, Monica Riva, and Alberto Guadagnini) -

We would like to thank Prof. Class for the careful and thorough reading of our manuscript and for his insightful comments and constructive suggestions that these have helped to improve the quality of the manuscript. Following is an itemized list of his comments (in italic) and our responses.

1) *This manuscript addresses the improvement of GSA (Global Sensitivity Analysis) by using newly introduced metrics based on the evaluation of the first four statistical moments: expectation value, variance, skewedness, tailedness. These metrics allow to extend the analysis beyond variance-based GSA into the details of the shape of the probability density function (pdf). It allows e.g. to detect when a certain model parameter particularly affects the asymmetry or the tailing of a pdf. The authors motivate and outline their idea in the context of GSA very well and nicely explain the expected benefits of their approach.*

   We thank Prof. Class for his positive assessment of our work.

2) *However, like always, there is no free lunch. The method has the disadvantage that it involves significantly more computational effort, this rendering likely impossible to perform for a complex hydrological scenario of practical relevance. The work-around proposed by Dell'Oca et al is the use of reduced-complexity models or surrogate models; in this case, they use the Polynomial Chaos Expansion technique, which can be viewed as an approximation of a target function by polynomials, where the degree of the polynomials determines (at least up to a certain value) the accuracy of the approximation.*
   Surrogate models like PCE require some smootheness in the targeted model output parameters with respect to the investigated paramters. Otherwise, discontinuities in the model output is difficult to reproduce. Therefore, I suppose, that this might involve the possibility that sophisticated GSA metrics become biased from errors introduced by the surrogate model. Thus, to give added value through several-moment-based GSA, we must first assure that the pdfs from the (surrogate) models are correct, i.e. the model represents the physics in all aspects. The manuscript addresses this issue quite well by some test cases, although I observe that all three test cases are relatively simple and do not provide huge challenges regarding possibly complex hydrological or geological features. The first test case is rather an academic exercise (which has, of course, value in itself), the second is an example where the results are definitely smooth in the parameter space; only the third one involves a heterogeneity, but still not very challenging for a polynomial approximation. I propose, maybe for future work, for example, a scenario where a fluid is injected into a geologic reservoir which has a fault zone in greater distance and where the response in terms of leakage to this fracture is rather a step-function. Would such a scenario be reflected properly by these new metrics? I guess that yes, but would the PCE provide the appropriate model for it? But clearly, the method proposed here is independent of the choice of the surrogate model.

We thank Prof. Class for pointing out this very relevant issue. As remarked by the Reviewer, in this manuscript we introduce novel metrics for global sensitivity analysis. These metrics can be evaluated making use of the complete model or (if the CPU time associated with the evaluation of the full model is too high) by a surrogate model. We also investigate the error associated with the evaluation of our novel metrics by replacing the complete system model through a gPCE. As proof of concept, we applied the proposed methodology to 3 (relatively simple) test cases. We agree with Prof. Class that any surrogate model (including gPCE) could fail in interpreting all the details of highly non-linear systems. The application of our methodology of analysis to more complex cases is envisioned as a future step. We will revise the opening statements of Section 3 of the manuscripts to highlight these relevant aspects.

3) *What if parameters are not uniformly distributed as assumed e.g. in 221-222? E.g. permeability in a fractured rock. How important is this assumption?*

Varying the probability density function (*pdf*) of uncertain model input parameters does not impact the definition of the novel metrics we propose. Otherwise, it may affect the actual results, depending on the test case considered. In the manuscript, we select uniform distributions for model parameters to mimic a scenario where the only information available is the expected range of variability of the parameters. We will highlight this issue in the revised manuscript.

4) *A given acceptable level of accuracy for the PCE-based approximation of the new indices requires increasing polynomial order with the order of the statistical moment. I can comprehend this statement in 3.3 (and in the conclusions with the careful wording "might be") from looking at the corresponding figures. But is there also some comprehensible reasoning or proof why this is the case? The authors are mathematicians and might be able to understand and explain this issue.*

A rigorous and general proof of the findings encapsulated in Figures 2 and 5 and evidenced by Prof. Class requires, for example, deriving (*a*) the analytical format of the probability density function (*pdf*) of a target model output on the basis of its gPCE based approximation at a given order *w*, and (*b*) the corresponding *pdf* associated with the full system model. We have shown a way to derive the former in a closed-form in a previous work (Riva et al., 2015, already referenced in the manuscript), at least for *w* = 2. With reference to the latter, one would need to formulate and solve (either analytically or numerically) appropriate (and exact) system equations satisfied by the *pdf* of interest or by its moments. This step is still an active area of research within which our group has considerable expertise. Approaches which are available in the literature always require approximations and specific assumptions, which are typically problem dependent. In this framework, a generalization of our findings is out of scope of the current study. Here, we rely on the direct solution of the full system model and the associated gPCE approximation to derive quantitative results for the examples considered. We will clarify these concepts in the revised manuscript.

References

Riva, M., Guadagnini, A. and Dell'Oca, A.: Probabilistic assessment of seawater intrusion under multiple sources of uncertainty, Adv. Water Resour., 75, 93-104, http://dx.doi.org/10.1016/j.advwatres.2014.11.002, 2015.

5) *I understood that the analysis helps better identifying the relative importance of individual parameters. There is enormous practical relevance for this, e.g. it would help to prioritize*

exploration efforts for a particular parameter when it becomes clear from the sensitivity analysis that knowledge about this parameter reduces uncertainty drastically. The authors might want to emphasize such examples a bit more prominently if they like.

We thank Prof. Class for this very interesting comment with which we fully agree. We will add an appropriate paragraph in the revised Introduction.

6) *In the first conclusion, line 475, I would write: "The CALCULATED sensitivity of a model output ..."*

We will modify the text accordingly.

7) *Very few language issues: 201-202: ... are affected by model uncertain parameters collected in x. Here is something wrong with the grammer, or I don't understand the meaning.*

The sentence will be reprahsed as "are affected by uncertain model parameters collected in the parameter vector x".

8) *326: maybe "characterize" is here not the right wording? What about "control"?*

The key point is to emphasize that the parameters we consider are affected by uncertainty. We will replace the wording 'characterize experimentally' by 'assess experimentally'.

Re: Response to the Comments of Dr. J. Bensabat on Manuscript HESSD-2017-90 (Moment-based Metrics for Global Sensitivity Analysis of Hydrological Systems by A. Dell'Oca, Monica Riva, and Alberto Guadagnini) -

We would like to thank Dr. Bensabat for the careful and thorough reading of our manuscript and for the insightful comments and constructive suggestions offered. It is our view that these have helped to improve the quality of the manuscript. Following is an itemized list of his comments (in italic) and our responses.

1) *This paper addresses the important topic of Sensitivity analysis of the output produced by hydrological models. The method is novel and provides a more mathematically rigorous framework for the evaluation of parameter sensitivity and a methodology for approximating the output produced by models in case they are demanding in terms of computational resources (PCE).*

    We thank Dr. Bensabat for his appreciaton of our work and his very positive comments.

2) *Three examples are investigated: 1) a synthetic case (the Ishigami function); 2) an analytical solution for seawater intrusion in a coastal aquifer (Pool and Carrera, 2011) and 3) A laboratory scale model of a solute transport. These three cases are all calculated and the relevant measures are presented.*
    Without any doubt this paper is substantial contribution and could lead to a better handling of complex hydrological systems

    We thank Dr. Bensabat for his positive assessment of our work.

3) *I would suggest to address a number of issues, which could make the paper attractive to an audience that is less familiar with the mathematical formulation of the method and more sensitive to its impact.*
    The presented cases are for either analytical solutions (cases 1 and 2) or small scale settings (case 3). Therefore it could be of value to discuss how this suggested methodology could be applied to hydrological problems (regional groundwater flow models, flow and transport models and or density dependent seawater intrusion), what would be the steps needed to be taken and what would be the implications in terms of required computational resources.

    We thank Dr. Bensabat for pointing out this very relevant issue. The diret application of our novel metrics for global sensitivity analysis (GSA) to field scale hydrological settings is envisioned as a future study. Such an application should be structured according to the steps detailed in Section 2. A critical limiting factor to any GSA approach is the associated computational burden. The latter is expected to increase according to two features associated with the conceptual and mathematical model used to describe the target variables of interest: (*a*) the complexity of the hydrological system (in terms of, e.g., hydrogeological heterogeneity, non-linear and/or transient effects), and/or (*b*) the number of uncertain model input parameters considered. According to the relative weight of these features, there can be some constraints to (*i*) perform the analysis by relying solely on the full system model, and (*ii*) construct a sufficiently accurate surrogate model through a number of full model runs which is affordable in terms of computational resources. We will revise the opening statements of Section 3 of the manuscripts to highlight these relevant aspects.

Moment-based Metrics for Global Sensitivity Analysis of Hydrological Systems

A. Dell'Oca[1], M. Riva[1,2], A. Guadagnini[1,2]

[1]Dipartimento di Ingegneria Civile e Ambientale (DICA), Politecnico di Milano, Piazza L. Da Vinci, 32, 20133 Milano, Italy

[2]Department of Hydrology and Atmospheric Sciences, University of Arizona, Tucson, Arizona, USA

Abstract

12   We propose new metrics to assist global sensitivity analysis, GSA, of hydrological and Earth

13   systems. Our approach allows assessing the impact of uncertain parameters on main features of the

14   probability density function, *pdf*, of a target model output, *y*. These include the expected value of *y*,

15   the spread around the mean and the degree of symmetry and tailedness of the *pdf* of *y*. Since reliable

16   assessment of higher order statistical moments can be computationally demanding, we couple our

17   GSA approach with a surrogate model, approximating the full model response at a reduced

18   computational cost. Here, we consider the generalized Polynomial Chaos Expansion (gPCE), other

19   model reduction techniques being fully compatible with our theoretical framework. We demonstrate

20   our approach through three test cases, including an analytical benchmark, a simplified scenario

21   mimicking pumping in a coastal aquifer, and a laboratory-scale conservative transport experiment.

22   Our results allow ascertaining which parameters can impact some moments of the model output *pdf*

23   while being uninfluential to others. We also investigate the error associated with the evaluation of our

24   sensitivity metrics by replacing the original system model through a gPCE. Our results indicate that

25   the construction of a surrogate model with increasing level of accuracy might be required depending

26   on the statistical moment considered in the GSA. Our approach is fully compatible with (and can

27   assist the development of) analysis techniques employed in the context of reduction of model

28   complexity, model calibration, design of experiment, uncertainty quantification and risk assessment.

1. Introduction

Our improved understanding of physical-chemical mechanisms governing hydrological processes at multiple space and time scales and the ever increasing power of modern computational resources are at the heart of the formulation of conceptual models which are frequently characterized by marked levels of sophistication and complexity. This is evident when one considers the spectrum of mathematical formulations and ensuing level of model parametrization rendering our conceptual understanding of given environmental scenarios (Willmann et al., 2006; Grauso et al., 2007; Koutsoyiannis, 2010; Wagener et al., 2010; Elshorbagy et al., 2010a,b; Wagener and Montanari, 2011; Hartmann et al., 2013; Herman et al., 2013; Förster et al., 2014; Paniconi and Putti, 2015). Model complexity can in turn exacerbate challenges associated with the need to quantify the way uncertainties associated with parameters of a given model propagate to target state variables.

In this context, approaches based on rigorous sensitivity analysis are valuable tools to improve our ability to (*i*) quantify uncertainty, (*ii*) enhance our understanding of the relationships between model input and outputs, and (*iii*) tackle the challenges of model- and data- driven design of experiments. These also offer insights to guide model simplification, e.g., by identifying model input parameters that have negligible effects on a target output. The variety of available sensitivity methodologies can be roughly subdivided into two broad categories, i.e., local and global approaches. Local sensitivity analyses consider the variation of a model output against variations of model input solely in the neighbourhood of a given set of parameters values. Otherwise, global sensitivity analysis (GSA) quantifies model sensitivity across the complete support within which model parameters can vary. Error measurements and/or lack of knowledge about parameters can be naturally accommodated in a GSA by specifying appropriate parameter intervals and evaluating sensitivity over the complete parameter space. Recent studies and reviews on available sensitivity analysis and approaches are offered by, e.g., Pianosi et al. (2016), Sarrazin et al. (2016), and Razavi and Gupta (2015).

Our study is framed in the context of GSA methods. A broadly recognized strategy to quantify global sensitivity of uncertain model parameters to model outputs relies on the evaluation of the

56 Sobol' indices (Sobol, 1993). These are typically referred to as variance-based sensitivity measures

57 because the output variance is taken as the metric upon which sensitivity is quantified. A key

58 limitation of a variance-based GSA is that the uncertainty of the output is implicitly considered to be

59 fully characterized by its variance. Relying solely on this criterion can provide an incomplete picture

60 of a system response to model parameters, also considering that probability densities of typical

61 hydrological quantities can be characterized by highly skewed and tailed distributions (e.g.,

62 Borgonovo et al., 2011). Recent studies (e.g., Krykacz-Hausmann, 2001; Borgonovo, 2007;

63 Borgonovo et al., 2011) introduce a sensitivity metric grounded on the complete probability density

64 function, *pdf,* of the model output. These so-called moment-independent analyses may suffer from

65 operational constraints, because a robust evaluation of the complete *pdf* may require a number of

66 model runs which is computationally unaffordable. The PAWN method developed by Pianosi and

67 Wagener (2015) attempts to overcome this limitation introducing a sensitivity metric based on the

68 cumulative density function, which can potentially be estimated more robustly than its associated *pdf*

69 for a given sample size.

70   It is clear that while a variance-based GSA can be favored for its conceptual simplicity and

71 ease of implementation and variance can be considered in some cases as an adequate proxy of the

72 spread around the mean, it does not yield a forthright quantification of the way variations of a

73 parameter can affect the structure of the *pdf* of a target model output. Otherwise, moment-independent

74 methodologies condense the entire *pdf* in only one index, somehow clouding our understanding of

75 how the structure of the *pdf* is affected by variations of each uncertain model parameter. Here, our

76 distinctive objective is to contribute to bridge the gap between these two types of GSA. We do so by

77 introducing theoretical elements and an implementation strategy which enable us to appraise

78 parameter sensitivity through the joint use of sensitivity indices based on four (statistical) moments

79 of the *pdf* of the model output: expected value, variance, skewness and kurtosis. The key idea at the

80 basis of this strategy is that linking parameter sensitivity to multiple statistical moments leads to

81 improved understanding of the way a given uncertain parameter can govern key features of the shape

82 of the *pdf* of desired model outputs, which is of interest in modern applications of hydrological and

83 Earth sciences.

84   Variance-based GSA has also been applied (*a*) to guide reduction of model complexity, e.g.,

85 by setting the value of a parameter which is deemed as uninfluential to the variance of a target model

86 output (e.g., Fu et al., 2012; Chu et al., 2015; Punzo et al., 2015), and (*b*) in the context of uncertainty

87 quantification (Saltelli et al., 2008; Pianosi et al., 2016; Colombo et al., 2016). Only limited attention

88 has been devoted to assess the relative effects of uncertain model parameters to the first four statistical

89 moment of the target model output. This information would complement a model complexity analysis

90 by introducing a quantification of the impact that conditioning the process on prescribed parameter

91 values would have on the first four statistical moment of the output. Our approach is based on the

92 joint use of multiple (statistical) moments for GSA. It enables us to address the following critical

93 questions: When can the variance be considered as a reliable proxy for characterizing model output

94 uncertainty? Which model parameter mostly affects asymmetry and/or the tailing behavior of a model

95 output *pdf*? Does a given model parameter have a marked role in controlling some of the first four

96 statistical moments of the model output, while being uninfluential to others? ==Addressing these==

97 ==questions would contribute to prioritize our efforts to characterize model parameters that are most==

98 ==relevant in affecting important aspects of model prediction uncertainty.==

99   Even as the richness of information content that a GSA grounded on the first four statistical

100 moments might carry can be a significant added value to our system understanding, it may sometimes

101 be challenging to obtain robust and stable evaluation of the proposed metrics for complex and

102 computationally demanding models. This can be especially true when considering higher-order

103 moments such as skewness and kurtosis. To overcome this difficulty, we cast the problem within a

104 computationally tractable framework by relying on the use of surrogate models, which mimic the full

105 model response with a reduced computational burden. Amongst the diverse available techniques to

106 construct a surrogate model (see, e.g., Razavi et al., 2012a,b), we exemplify our approach by

107 considering the generalized Polynomial Chaos Expansion (gPCE) that has been successfully applied

108   to a variety complex environmental problems (Sudret, 2008; Ciriello et al., 2013; Formaggia et al.,

109   2013; Riva et al., 2015; Gläser et al., 2016), other model reduction techniques being fully compatible

110   with our GSA framework. In this context, we also investigate the error associated with the evaluation

111   of the sensitivity metrics we propose by replacing the original (full) system model through the

112   selected surrogate model for three test cases. These include a widely employed analytical benchmark,

113   a pumping scenario in a coastal aquifers, and a laboratory-scale transport setting. The remainder of

114   the work is organized as follows. Section 2 presents our theoretical framework and developments.

115   Section 3 illustrates our results for the three test cases indicated above and conclusions are drawn in

116   Section 4.

117   **2. Theoretical framework**

118   We start by recalling the widely used variance-based GSA metrics in Section 2.1. These allow

119   quantifying the contribution of each uncertain parameter to the total variance of a state variable of

120   interest. We also provide a brief overview of the generalized Polynomial Chaos Expansion (gPCE)

121   technique, which we use to construct a surrogate of the full system model. We then illustrate in

122   Section 2.2 the theoretical developments underlying our approach and introduce novel GSA indices.

123   **2.1 Sobol' indices for variance-based GSA and generalized Polynomial Chaos Expansion**

124   We consider a target system state variable, y, which depends on N random parameters. These

125   are collected in vector $\boldsymbol{x} = (x_1, x_2, \ldots, x_N)$ and defined in the parameter space $\Gamma = \Gamma_1 \times \Gamma_2 \times \ldots \Gamma_N$,

126    $\Gamma_i = [x_{i,\min}, x_{i,\max}]$ being the support of the i-th random variable x_i. Variance-based GSA approaches

127   consider variance as the sole metric to quantify the contribution of each uncertain parameter to the

128   uncertainty of y. Iman and Hora (1990) introduce the following index

129    $HI_{x_i} = V[y] - E\big[V[y \,|\, x_i]\big] = V\big[E[y \,|\, x_i]\big],$ (1)

130    $E[-]$ and $V[-]$ respectively denoting expectation and variance operators. Index HI_{x_i} quantifies the

131   expected reduction of variance due to knowledge of x_i (the notation $|\, x_i$ in Eq. (1) indicates

132   conditioning on x_i). A similar measure is offered by the widely used Sobol' indices (Sobol, 1993).

133   These have been defined starting from the Hoeffendig/Sobol decomposition (see, e.g., Sobol, 1993,

134   Le Maître and Knio, 2010) of $y(\boldsymbol{x})$ when $\boldsymbol{x}$ is a collection of independent random variables as

$$y(\boldsymbol{x}) = y_0 + \sum_{x_i=1}^{N} y_{x_i}(x_i) + \sum_{x_i < x_j} y_{x_i,x_j}(x_i, x_j) + ... + y_{x_1,x_2,...,x_N}(x_1, x_2, ..., x_N), \tag{2}$$

135

136   where

$$y_0 = \int_{\Gamma} y(\boldsymbol{x})\rho_{\Gamma\boldsymbol{x}} \, d\boldsymbol{x},$$

137
$$y_{x_i}(x_i) = \int_{\Gamma \sim x_i} y(\boldsymbol{x})\rho_{\Gamma \sim x_i} d\boldsymbol{x}_{\sim x_i} - y_0, \tag{3}$$

$$y_{x_i,x_j}(x_i, x_j) = \int_{\Gamma \sim x_i,x_j} y(\boldsymbol{x})\rho_{\Gamma \sim x_i,x_j} d\boldsymbol{x}_{\sim x_i,x_j} - y_{x_i}(x_i) - y_{x_j}(x_j) - y_0,$$

138   and so on, $\rho_{\Gamma\boldsymbol{x}}$ being the *pdf* of $\boldsymbol{x}$. The integral $\int_{\Gamma \sim x_i} y(\boldsymbol{x})\rho_{\Gamma \sim x_i} d\boldsymbol{x}_{\sim x_i}$ in Eq. (3) represents integration

139   of $y(\boldsymbol{x})$ over the space of all entries of vector $\boldsymbol{x}$ excluding x_i, $\rho_{\Gamma \sim x_i}$ being the corresponding *pdf*. The

140   Sobol' index $S_{x_{i_1},x_{i_2},...,x_{i_s}}$ is associated with the mixed effect of $x_{i_1}, x_{i_2}, ..., x_{i_s}$ on the variance of $y(\boldsymbol{x})$,

141    $V[y]$, and can be computed as

$$S_{x_{i_1},x_{i_2},...,x_{i_s}} = \frac{1}{V[y]} \int_{\Gamma_{x_{i_1},x_{i_2},...,x_{i_s}}} y_{x_{i_1},x_{i_2},...,x_{i_s}}(x_{i_1}, x_{i_2}, ..., x_{i_s}) \, \rho_{\Gamma x_{i_1},x_{i_2},...x_{i_s}} dx_{i_1}...dx_{i_s}. \tag{4}$$

142

143   The principal and total Sobol' indices are respectively defined as

$$S_{x_i} = \frac{1}{V[y]} \int_{\Gamma_{x_i}} \left[y_{x_i}(x_i) \right]^2 \rho_{\Gamma x_i} dx_i, \tag{5}$$

144

$$S_{x_i}^T = S_{x_i} + \sum_{x_j} S_{x_i,x_j} + \sum_{x_j,x_k} S_{x_i,x_j,x_k} + ... \tag{6}$$

145

146   Note that S_{x_i} describes the relative contribution to $V[y]$ due to variability of only x_i. Otherwise, $S_{x_i}^T$

147   quantifies the total contribution of x_i to $V[y]$, including all terms where x_i appears. In other words,

148    $S_{x_i}^T$ also includes interactions between x_i and the remaining uncertain parameters, collected in vector

149    $x_{\sim x_i}$. Note that according to Eq.s (1)-(2) and Eq. (5)

150
$$S_{x_i} = \frac{V[E[y \mid x_i]]}{V[y]} = \frac{HI_{x_i}}{V[y]},$$
        (7)

151   i.e., the principal Sobol' index represents the relative expected reduction of process variance due to

152   knowledge of (or conditioning on) a parameter. Sobol' indices are commonly evaluated via Monte

153   Carlo quadrature schemes that can be markedly demanding in terms of computational time, especially

154   for complex and highly non-linear settings. Relying on a generalized Polynomial Chaos Expansion,

155   gPCE, as a surrogate of the full mathematical model of the system (Ghanem and Spanos, 1991; Xiu

156   and Karniadakis, 2002; Le Maitre and Knio, 2010; Formaggia et al., 2013; Ciriello et al., 2013; Riva

157   et al., 2015) allows reducing the computational burden associated with GSA techniques. The process

158    $y(x)$ is represented as a linear combination of multivariate polynomials, $\psi_p(x)$, i.e.,

159
$$y(x) \cong \beta_0 + \sum_{i=1}^{N} \sum_{p \in \Im_i} \beta_p \psi_p(x) + \sum_{i=1}^{N} \sum_{j=1}^{N} \sum_{p \in \Im_{i,j}} \beta_p \psi_p(x) + ...,$$
$$\psi_p(x) = \prod_{i=1}^{N} \psi_{i,p_i}(x_i), \quad \beta_p = \int_{\Gamma} y(x) \psi_p(x) \rho_{\Gamma x} \, dx,$$
        (8)

160   where $p = \{p_1, ..., p_N\} \in N^N$ is a multi-index expressing the degree of each univariate polynomial,

161    $\psi_{i,p_i}(x_i)$; β_p are the gPCE coefficients; $\Im_i$ contains all indices such that only the i-th component

162   does not vanish; $\Im_{i,j}$ contains all indices such that only the i-th and j-th components are not zero, and

163   so on. Note that $\beta_0 \equiv y_0$, i.e., β_0 is the unconditional mean of $y(x)$. Finally, the Sobol' indices Eq.s

164   (4)-(5) and the variance of $y(x)$ can be computed from Eq. (8) as

165
$$S_{x_{i_1}, ..., x_{i_s}} = \frac{1}{V[y]} \sum_{p \in \Im_{i_1, ..., i_s}} \beta_p^2, \qquad S_{x_i} = \frac{1}{V[y]} \sum_{p \in \Im_i} \beta_p^2, \qquad V[y] = \sum_{p \in N^N} \beta_p^2 - \beta_0^2.$$
        (9)

166   **2.2 New metrics for multiple-moment GSA**

167   We introduce new metrics to quantify the expected relative change of main features of the *pdf*

168   of *y* due to variability of model input parameters. In contrast with traditional variance-based GSA

169   techniques of the kind described in Section 2.1, we quantify changes in the *pdf* of *y* through its first

170   four statistical moments, i.e., mean, $E[y]$, variance, $V[y]$, skewness, $\gamma[y]$, and kurtosis, $k[y]$. The

171   latter is an indicator of the behavior of the tails of the *pdf* of *y* and is particularly useful in the context

172   of risk analysis, $\gamma[y]$ quantifying the asymmetry of the *pdf* of *y*.

173   The effect of changes of $\boldsymbol{x}$ on the mean of *y* cannot be systematically analyzed by the metrics

174   currently available in the literature. We therefore introduce the following quantity

175    $$AMAE_{x_i} = \begin{cases} \dfrac{1}{|y_0|} \displaystyle\int_{\Gamma_{x_i}} |y_0 - E[y\,|\,x_i]| \rho_{\Gamma x_i} dx_i \;=\; \dfrac{1}{|y_0|} E\big[|y_0 - E[y\,|\,x_i]|\big] & if \quad y_0 \neq 0 \\[2mm] \displaystyle\int_{\Gamma_{x_i}} |E[y\,|\,x_i]| \rho_{\Gamma x_i} dx_i \;=\; E\big[|E[y\,|\,x_i]|\big] & if \quad y_0 = 0 \end{cases} \tag{10}$$

176   y_0 being defined in Eq. (3). Extension of Eq. (10) to consider the joint effect of $x_{i_1}, x_{i_2}, ..., x_{i_s}$ on the

177   mean of *y* is straightforward, leading to the following index

178    $$AMAE_{x_{i_1},...,x_{i_s}} = \begin{cases} \dfrac{1}{|y_0|} \displaystyle\int_{\Gamma_{x_{i1},...,x_{is}}} \left|y_0 - E[y\,|\,x_{i_1},...,x_{i_s}]\right| \rho_{\Gamma x_{i1},...,x_{is}} dx_{i_1}...dx_{i_s} \\[2mm] \qquad = \dfrac{1}{|y_0|} E\big[\left|y_0 - E[y\,|\,x_{i_1},...,x_{i_s}]\right|\big] & if \quad y_0 \neq 0 \\[2mm] \displaystyle\int_{\Gamma_{x_{i1},...,x_{is}}} \left|E[y\,|\,x_{i_1},...,x_{i_s}]\right| \rho_{\Gamma x_{i1},...,x_{is}} dx_{i_1}...dx_{i_s} = E\big[\left|E[y\,|\,x_{i_1},...,x_{i_s}]\right|\big] & if \quad y_0 = 0 \end{cases} \tag{11}$$

179   Note that index $AMAE_{x_i}$ quantifies the expected relative variation of the mean of *y* due to variations

180   of only x_i, while $AMAE_{x_{i_1},...,x_{i_s}}$ also includes all interactions amongst parameters $x_{i_1}, x_{i_2}, ..., x_{i_s}$.

181   Along the same lines, we introduce the following index

182    $$AMAV_{x_i} = \frac{1}{V[y]} \int_{\Gamma_{x_i}} |V[y] - V[y\,|\,x_i]| \rho_{\Gamma x_i} dx_i \;=\; \frac{E\big[|V[y] - V[y\,|\,x_i]|\big]}{V[y]}, \tag{12}$$

183   quantifying the relative expected discrepancy between unconditional and conditional (on x_i) process

184 variance. Note that Eq. (12) does not generally coincide with the principal Sobol' index S_{x_i} in Eq.

185 (7) that quantifies the expected relative reduction of the variance due to knowledge of x_i (or, in other

186 words, the relative contribution to the variance arising from uncertainty in x_i). Index $AMAV_{x_i}$

187 reduces to S_{x_i} only if the conditional variance, $V[y | x_i]$, is always (i.e., for each value of x_i) smaller

188 than (or equal to) its unconditional counterpart $V[y]$. The difference between $AMAV_{x_i}$ and S_{x_i}, as

189 well as advantages of using $AMAV_{x_i}$, will be elucidated through the numerical examples illustrated

190 in Section 3. Extension of Eq. (12) to consider the joint effect of $x_{i_1}, x_{i_2}, ..., x_{i_s}$ reads

$$
\begin{aligned}
AMAV_{x_{i_1} ..., x_{i_s}} &= \frac{1}{V[y]} \int_{\Gamma_{x_{i_1} ..., x_{i_s}}} \left| V[y] - V[y | x_{i_1}, ..., x_{i_s}] \right| \rho_{\Gamma_{x_{i1}, ..., x_{is}}} dx_{i_1} ... dx_{i_s} \\
&= \frac{1}{V[y]} E\left[\left| V[y] - V\left[y | x_{i_1}, ..., x_{i_s} \right] \right| \right]
\end{aligned}
$$
191   (13)

192 Index $AMAV_{x_{i_1}, ..., x_{i_s}}$ quantifies the expected relative discrepancy between $V[y]$ and the variance of

193 the process conditional to joint knowledge of $x_{i_1}, x_{i_2}, ..., x_{i_s}$.

194   We then quantify the relative expected discrepancy between unconditional, $\gamma[y]$, and

195 conditional, $\gamma[y | x_i]$, skewness through the index

$$
AMA\gamma_{x_i} = \begin{cases} \frac{1}{|\gamma[y]|} \int_{\Gamma_{x_i}} \left| \gamma[y] - \gamma[y | x_i] \right| \rho_{\Gamma x_i} dx_i = \frac{1}{|\gamma[y]|} E\left[\left| \gamma_y - \gamma[y | x_i] \right| \right] & \text{if } \gamma_y \neq 0 \\ \int_{\Gamma_{x_i}} \left| \gamma[y | x_i] \right| \rho_{\Gamma x_i} dx_i = E\left[\left| \gamma[y | x_i] \right| \right] & \text{if } \gamma_y = 0 \end{cases}
$$
196   (14)

197 Extension of Eq. (14) to consider the joint effect of $x_{i_1}, x_{i_2}, ..., x_{i_s}$ gives

$$
AMA\gamma_{x_{i_1}, ..., x_{i_s}} = \begin{cases} \frac{1}{|\gamma[y]|} \int_{\Gamma_{x_{i_1}, ..., x_{i_s}}} \left| \gamma[y] - \gamma[y | x_{i_1}, ..., x_{i_s}] \right| \rho_{\Gamma_{x_{i1}, ..., x_{is}}} dx_{i_1} ... dx_{i_s} \\ \qquad = \frac{1}{|\gamma[y]|} E\left[\left| \gamma[y] - \gamma\left[y | x_{i_1}, ..., x_{i_s} \right] \right| \right] & \text{if } \gamma[y] \neq 0 \\ \int_{\Gamma_{x_{i_1}, ..., x_{i_s}}} \left| \gamma[y | x_{i_1}, ..., x_{i_s}] \right| \rho_{\Gamma_{x_{i1}, ..., x_{is}}} dx_{i_1} ... dx_{i_s} = E\left[\left| E[y | x_{i_1}, ..., x_{i_s}] \right| \right] & \text{if } \gamma[y] = 0 \end{cases}
$$
198   (15)

199   The relative variation of the kurtosis of y due to variations of a parameter x_i or of the

200   parameter set $x_{i_1}, x_{i_2}, ..., x_{i_s}$ can be respectively quantified through

201    $$AMAk_{x_i} = \frac{1}{k[y]} \int_{\Gamma_{x_i}} |k[y] - k[y \mid x_i]| \rho_{\Gamma_{x_i}} dx_i = \frac{1}{k[y]} E\Big[|k[y] - k[y \mid x_i]|\Big], \tag{16}$$

202    $$\begin{aligned} AMAk_{x_{i_1}, ..., x_{i_s}} &= \frac{1}{k[y]} \int_{\Gamma_{x_{i_1}, ..., x_{i_s}}} |k[y] - k[y \mid x_{i_1}, ..., x_{i_s}]| \rho_{\Gamma_{x_{i1}, ..., x_{is}}} dx_{i_1} ... dx_{i_s} \\ &= \frac{1}{k[y]} E\Big[|k[y] - k[y \mid x_{i_1}, ..., x_{i_s}]|\Big] \end{aligned} \tag{17}$$

203   Relying jointly on Eq.s (10)-(17) enables one to perform a comprehensive GSA of the target

204   process $y(\boldsymbol{x})$ quantifying the impact of $\boldsymbol{x}$ on the first four (statistical) moments of the *pdf* of $y(\boldsymbol{x})$.

205   This strategy yields information about the way important elements of the distribution of $y(\boldsymbol{x})$, such

206   as mean, spread around the mean, symmetry, and tailedness, are affected by uncertain model

207   parameters collected in the parameter vector $\boldsymbol{x}$. This analysis is not feasible through a classical

208   variance- based GSA.

209   Calculation of the indices we propose entails evaluation of conditional moments of $y(\boldsymbol{x})$. This

210   step can be computationally very demanding. Along the lines of our discussion about Sobol' indices

211   in Section 2.1, the new metrics Eq.s (10)-(17) can be evaluated via a surrogate model, as we illustrate

212   through our examples in Section 3.

213   **3. Illustrative Examples**

214   The theoretical framework introduced in Section 2 is here applied to three diverse testbeds:

215   (*a*) the Ishigami function, which constitutes an analytical benchmark typically employed in GSA

216   studies; (*b*) a pumping scenario in a coastal aquifer, where the state variable of interest is the critical

217   pumping rate, i.e. the largest admissible pumping rate to ensure that the extraction well is still not

218   contaminated by seawater; and (*c*) a laboratory-scale setting associated with non-reactive transport in

219   porous media. In the first two examples the relatively low computational costs associated with the

220   complete mathematical description of the target outputs enables us to assess also the error associated

221 with the evaluation of indices Eq. (10), Eq. (12), Eq. (14) and Eq. (16) through a gPCE representation

222 of the output. In the third case, due to the complexity of the problem and the associated computational

223 costs, we relay on the gPCE representation for the target quantity of interest. We emphasize that the

224 use of a gPCE as a surrogate model is here considered only as an example, our GSA approach being

225 fully compatible with any full model and/or model order reduction technique. A critical limiting factor

226 to our and any GSA approach could be the associated computational burden. The latter is expected to

227 increase according to the following two features, which are mainly associated with the conceptual

228 and mathematical model used to describe the target variables of interest: (*a*) the complexity of the

229 hydrological system (in terms of, e.g., hydrogeological heterogeneity, non-linearity and/or transient

230 effects), and/or (*b*) the number of uncertain model input parameters considered. According to the

231 relative weight of these features, some computational constraints might arise limiting our ability to

232 (*i*) perform the analysis by relying exclusively on the full system model, or (*ii*) construct a sufficiently

233 accurate surrogate model through a number of full model runs that can be affordable in terms of

234 available computational resources. Application of our GSA methodology to scenarios of increased

235 level of complexity will be the subject of a future study.

236   In all of the above scenarios, uncertain parameters x_i collected in $\boldsymbol{x}$ are considered as

237 independent and identically distributed, *i.i.d.*, random variables, each characterized by a uniform

238 distribution within the interval $\Gamma_i = \left[x_{i,\min}, x_{i,\max} \right]$. Note that varying the *pdf* of the uncertain model

239 input parameters does not impact the definition of the GSA indices proposed in Section 2. Otherwise,

240 it may affect the actual results, depending on the test case considered. All results are grounded on

241 5×10^5 Monte Carlo realizations, enabling convergence of all statistical moments analyzed. Series

242 appearing in the gPCE Eq. (8) are evaluated up to a given order of truncation in all three examples.

243 Here, we apply the total-degree rule and construct a polynomial of order w through a sparse grid

244 technique (see, e.g., Formaggia et al., 2013 and references therein). We then analyze the way the

245 selected order w influences the results. Note that the optimal choice of the polynomial $\psi_p(\boldsymbol{x})$ in Eq.

246 (8) depends on the *pdf* of the random variables collected in $\boldsymbol{x}$ (Xiu and Karniadakis, 2002). In our

247 exemplary settings we use the multidimensional Legendre polynomials which are orthonormal with

248 respect to the uniform *pdf*.

3.1 Ishigami function

250   The non-linear and non-monotonic Ishigami function

251 $$y(\boldsymbol{x}) = ISH(\boldsymbol{x}) = \sin(2\pi x_1 - \pi) + a\sin^2(2\pi x_2 - \pi) + b(2\pi x_3 - \pi)^4 \sin(2\pi x_1 - \pi) \tag{18}$$

252 is widely used in the literature (e.g., Homma and Saltelli, 1996; Chun et al., 2000; Borgonovo, 2007;

253 Sudret, 2008; Crestaux et al., 2009; Borgonovo et al. 2011) to benchmark GSA methods. Here, x_i (i

254 = 1, 2, 3) are *i.i.d.* random variables uniformly distributed within the interval [0, 1]. Unconditional

255 mean $E[ISH]$, variance, $V[ISH]$, skewness, $\gamma[ISH]$, and kurtosis, $k[ISH]$, of Eq. (18) can be

256 evaluated analytically as

257 $$E[ISH] = \frac{a}{2}, \qquad V[ISH] = \frac{1}{2} + \frac{a^2}{8} + b\pi^4\left(\frac{1}{5} + \frac{b\pi^4}{18}\right), \qquad \gamma[ISH] = 0, \tag{19a}$$

258 $$k[ISH] = \frac{1}{2V^2[ISH]}\left\{\frac{3}{4} + b\pi^4\left[\frac{3}{5} + b\pi^4\left(\frac{1}{2} + 3b\pi^4\left(\frac{1}{13} + \frac{\pi^4 b}{68}\right)\right)\right] + \frac{3}{2}a^2\left[\frac{1}{2} + \frac{a^2}{32} + \pi^4 b\left(\frac{1}{5} + \frac{\pi^4 b}{18}\right)\right]\right\}.$$

259 $$\tag{19b}$$

260 Equation (19) reveals that the unconditional *pdf* of *ISH* is symmetric with tails that increase with |*b*|

261 and decrease with |*a*|, as quantified by $k[ISH]$. The conditional mean $E[ISH \mid x_i]$, variance

262 $V[ISH \mid x_i]$, skewness $\gamma[ISH \mid x_i]$ and kurtosis $k[ISH \mid x_i]$ can be evaluated analytically as

263 $$E[ISH \mid x_1] = \frac{a}{2} - \frac{1}{5}(5 + b\pi^4)\sin(2\pi x_1), \quad E[ISH \mid x_2] = a\sin^2(2\pi x_2), \quad E[ISH \mid x_3] = \frac{a}{2}, \tag{20}$$

264
$$V[ISH \mid x_1] = \frac{a^2}{8} + \frac{8b^2\pi^8}{225}(1 - \cos(4\pi x_1)), \qquad V[ISH \mid x_2] = \frac{1}{2} + b\pi^4\left(\frac{1}{5} + \frac{b}{18}\pi^4\right),$$
$$V[ISH \mid x_3] = \frac{a^2}{8} + \frac{1}{2}\left(1 + b\pi^4(1 - 2x_3)^4\right)^2,$$
$$\tag{21}$$

265 $$\gamma\left[ISH \mid x_1\right] = -\frac{128b^3\pi^{12}\sin^3\left(2\pi x_1\right)}{4875\left(V\left[ISH \mid x_1\right]\right)^{3/2}}, \qquad \gamma\left[ISH \mid x_2\right] = 0, \qquad ISH\left[y \mid x_3\right] = 0, \quad (22)$$

266 $$k\left[ISH \mid x_1\right] = \frac{1}{V^2\left[ISH \mid x_1\right]}\left\{\frac{3}{128}a^4 + \frac{4}{75}b^2\pi^8\sin^2\left(2\pi x_1\right)\left[a^2 + \frac{1849}{5525}b^2\pi^8\sin^2\left(2\pi x_1\right)\right]\right\},$$

$$k\left[ISH \mid x_2\right] = \frac{1}{2V^2\left[ISH \mid x_2\right]}\left\{\frac{3}{4} + b\pi^4\left[\frac{3}{5} + b\pi^4\left(\frac{1}{2} + 3b\pi^4\left(\frac{1}{13} + \frac{1}{68}b\pi^4\right)\right)\right]\right\}, \qquad (23)$$

$$k\left[ISH \mid x_3\right] = \frac{3}{128V^2\left[ISH \mid x_3\right]}\left\{a^4 + 16\left(1 + b\pi^4\left(1 - 2x_3\right)^4\right)^2\left[a^2 + \left(1 + b\pi^4\left(1 - 2x_3\right)^4\right)^2\right]\right\}.$$

267 For the sole purpose of illustrating our approach, here and in the following we set $a = 5$ and $b = 0.1$,

268 which corresponds to $E\left[ISH\right] = 2.50$, $V\left[ISH\right] = 10.84$ and $k\left[ISH\right] = 4.18$. Figure 1 depicts the

269 first four moments of ISH conditional to values of x_1 (blue curves), x_2 (red curves) and x_3 (green

270 curves) within the parameter space. The corresponding unconditional moments (black curves) are

271 also depicted for completeness.

272 Comparing Eq. (19a) and Eq. (20), it is seen that $E\left[ISH \mid x_3\right]$ coincides with its unconditional

273 counterpart $E\left[ISH\right]$, indicating that conditioning on any value of x_3 does not impact the mean of

274 ISH. Otherwise, setting x_1 or x_2 to a given value clearly affects the mean of ISH in a way which is

275 governed by Eq. (20) and shown in Fig. 1a. It is clear from Eq. (20) that $E\left[ISH \mid x_2\right]$ has a higher

276 frequency of oscillation within Γ_{x_2} than has $E\left[ISH \mid x_1\right]$ within Γ_{x_1}. The global index in Eq. (10)

277 can be evaluated analytically as

278 $$AMAE_{x_1} = \frac{4}{a\pi}\left|1 + \frac{b}{5}\pi^4\right|, \qquad AMAE_{x_2} = \frac{2}{\pi}\frac{|a|}{a}, \qquad AMAE_{x_3} = 0. \qquad (24)$$

279 Note that $AMAE_{x_2}$ does not depend on specific values of a and b.

280 Equation (21) shows that all random model parameters influence the variance of ISH, albeit

281 to different extents, as also illustrated in Fig. 1b. Note that $V\left[ISH \mid x_2\right]$ is always smaller than

282 $V\left[ISH\right]$ (compare Eq. (19a) and Eq. (21)) and does not depend on x_2, i.e., conditioning ISH on x_2

283   reduces the process variance regardless the conditioning value. Otherwise, $V\left[ISH \mid x_3\right]$ can be

284   significantly larger or smaller than its unconditional counterpart. Table 1 lists values of $AMAV_{x_i}$ (x_i

285    $= x_1,\ x_2,\ x_3$) computed via Eq. (12) with the a and b values selected for our demonstration. The

286   principal Sobol' indices (Sudret, 2008)

287    $$S_{x_1} = \frac{\left(5 + b\pi^4\right)^2}{50\,V\left[ISH\right]}, \qquad\qquad S_{x_2} = \frac{a^2}{8\,V\left[ISH\right]}, \qquad\qquad S_{x_3} = 0, \qquad (25)$$

288   are also listed for completeness. As expected, values of $AMAV_{x_i}$ listed in Table 1 suggest that

289   conditioning on x_3 has the strongest impact on the variance of *ISH*, followed by x_1 and x_2. Note that

290    $S_{x_3} = 0$, a result which might be interpreted as a symptom that *ISH* is insensitive to x_3. The apparent

291   inconsistency between the conclusions which could be drawn by analysing $AMAV_{x_3}$ and S_{x_3} is

292   reconciled by the observation that the function $V\left[ISH\right] - V\left[ISH \mid x_3\right]$ can be positive and negative in

293   a way that its integration over Γ_{x_3} vanishes (see also Fig. 1b). Therefore, the mean reduction of the

294   variance of *ISH* due to knowledge of (or conditioning on) x_3 is zero. It is remarked that this

295   observation does not imply that the variance of *ISH* does not vary with x_3, as clearly highlighted by

296   Fig. 1b and quantified by $AMAV_{x_3}$.

297   The symmetry of the *pdf* of *ISH* is not affected by conditioning on x_2 or x_3, as demonstrated

298   by Eq. (22). Otherwise, $\gamma\left[ISH \mid x_1\right]$ is left (or right) skewed when x_1 is smaller (or larger) than 0.5,

299   as dictated by Eq. (22) and shown in Fig. 1c.

300   The conditional kurtosis $k\left[ISH \mid x_2\right]$ does not depend on the conditioning value x_2 (see Eq.

301   (23)). We then note that this conditional moment is always larger than (or equal to) its unconditional

302   counterpart $k\left[ISH\right]$, regardless the particular values assigned to a and b, as we verified through

303   extensive numerical tests. This result implies that the *pdf* of *ISH* conditional on x_2 is characterized

by tails which are heavier than those of its unconditional counterpart. Figure 1d reveals that

$k\left[ISH \mid x_1\right]$ and $k\left[ISH \mid x_3\right]$ are smaller than $k\left[ISH\right]$ for the values of a and b implemented in this

example. Table 1 lists the resulting values of $AMAk_{x_i}$ ($x_i = x_1, x_2, x_3$) for the selected a and b

values.

We close this part of the study by investigating the error which would arise when one evaluates

our GSA indices by replacing ISH through a gPCE surrogate model. We do so on the basis of the

absolute relative error

$$e_j = \begin{cases} \left|\dfrac{j_{gPCE} - j_{full\,model}}{j_{full\,model}}\right| & if \quad j_{full\,model} \neq 0 \\ \left|j_{gPCE} - j_{full\,model}\right| & if \quad j_{full\,model} = 0 \end{cases}, \tag{26}$$

where $j = AMAE_{x_i}$, $AMAV_{x_i}$, $AMA\gamma_{x_i}$ or $AMAk_{x_i}$ ($x_i = x_1, x_2, x_3$); the subscripts *full model* and

gPCE respectively indicate that quantity j is evaluated via Eq. (18) or through a gPCE surrogate

model, constructed as outlined in Section 2.1. Figure 2 depicts Eq. (26) versus the total degree w of

the gPCE. Note that the lower limit of the vertical axis of Fig. 2 is set to 0.001% for convenience of

graphical representation. Approximation errors associated with GSA indices related to the mean,

$AMAE_{x_i}$, rapidly approach zero as w increases. Note that $e_{AMAE_{x_3}}$ is smaller than 0.001% for all tested

values of w and it is therefore not included in Fig. 2a. Values of e_j linked to $AMAV_{x_i}$, $AMA\gamma_{x_i}$ and

$AMAk_{x_i}$ do not show a consistently decreasing trend until $w \geq 5$. Values of e_j associated with the

variance, skewness and kurtosis decrease with approximately the same average linear rate (in log-log

scale) for the largest w considered (Fig.s 2b, 2c and 2d). This example reinforces the need for reliably

testing the accuracy of a gPCE-based model approximation as a function of the total degree desired,

depending on the statistical moment of interest. ==Note that a generalization of our findings about the==

==error (26) is outside the scope of the current study. This would require the derivation of (*a*) the==

==analytical format of the *pdf* of a target model output through its gPCE based approximation at a given==

3.2 Critical Pumping Rate in Coastal Aquifers

The example we consider here is taken from the study of Pool and Carrera (2011) related to the analysis of salt water contamination of a pumping well operating in a homogenous confined coastal aquifer of uniform thickness $b^{'}$. The setting is sketched in Fig. 3. A constant discharge, $Q_w^{'}$ [$L^3\,T^{-1}$], is pumped from a fully penetrating well located at a distance $x_w^{'}$ [L] from the coastline and a constant freshwater flux, $q_f^{'}$ [$L\,T^{-1}$], flowing from the inland to the coastline, is set. Pool and Carrera (2011) introduced a dimensionless well discharge $Q_w = Q_w^{'} / (b^{'} x_w^{'} q_f^{'})$ and defined the critical pumping rate Q_c as the value of Q_w at which a normalized solute concentration monitored at the well exceeds 0.1%. A key result of the study of Pool and Carrera (2011) is that Q_c can be approximated through the following implicit equation

$$\lambda_D = 2\left[1 - \frac{Q_c}{\pi}\right]^{1/2} + \frac{Q_c}{\pi} \ln \frac{1 - \left(1 - Q_c / \pi\right)^{1/2}}{1 + \left(1 - Q_c / \pi\right)^{1/2}} \qquad \text{with} \qquad \lambda_D = \frac{\Delta \rho^{'}}{\rho_f^{'}} \frac{1 - \left(Pe_T\right)^{-1/6}}{x_w J}. \tag{27}$$

Here, $x_w = x_w^{'} / b^{'}$; $J = q_f^{'} / K$; $Pe_T = b^{'} / \alpha_T^{'}$; K [$L\,T^{-1}$] is the uniform hydraulic conductivity; $\alpha_T^{'}$ [L] is transverse dispersivity; $\Delta \rho^{'} = \rho_s^{'} - \rho_f^{'}$, $\rho_f^{'}$ and $\rho_s^{'}$ being fresh- and salt-water densities, respectively. The quantity Pe_T is a measure of the intensity of dispersive effects, *J* is the natural head gradient of the incoming freshwater, and x_w is the dimensionless distance of the well from the coastline. Pool and Carrera (2011) demonstrated the accuracy of Eq. (27) in predicting the critical pumping rate when $\lambda_D \in (0-10]$. Additional details about the problem setting, boundary and initial conditions, as well as geometrical configuration of the system can be found in Pool and Carrera

348 (2011). Here, we focus on the main result of Eq. (27) which represents the complete mathematical

349 description of the problem we analyze. We perform a sensitivity analysis of Q_c with respect to Pe_T

350 , J, and x_w. While the first two quantities are difficult to assess experimentally in practical

351 applications, the well location can be considered as an operational/design variable. Table 2 lists the

352 intervals of variation we consider for Pe_T, J and x_w. These are designed to (*a*) resemble realistic

353 field values and (*b*) obey the above mentioned constraint about λ_D.

354   Numerical evaluation of the first four unconditional statistical moment of Q_c yields a mean

355 value $E[Q_c] = 1.65$, variance $V[Q_c] = 0.17$, skewness $\gamma[Q_c] = -0.30$ (which indicates a light

356 asymmetry in the *pdf*), and kurtosis $k[Q_c] = 2.51$ (i.e., *pdf* tails decrease faster than those of a

357 Gaussian distribution). Figure 4 depicts the first four moments of Q_c conditional to values of Pe_T

358 (blue curves), J (green curves), and x_w (red curves) within the parameter space. The corresponding

359 unconditional moments (black curves) are also depicted for completeness. Note that each parameter

360 interval of variation has been normalized to span the range [0, 1] for graphical representation

361 purposes. Table 3 lists the values of indices $AMAE_{x_i}$ $AMAV_{x_i}$, S_{x_i}, $AMA\gamma_{x_i}$ and $AMAk_{x_i}$ ($x_i = $

362 Pe_T, J, x_w) associated with Q_c. As in our first example, it is clear that sensitivity of Q_c with respect

363 to Pe_T, J, x_w depends on the statistical moment of interest.

364   Inspection of Fig. 4a reveals that the mean of Q_c is more sensitive to conditioning on J or x_w

365 than to conditioning on Pe_T. Note that increasing Pe_T, i.e., considering advection-dominated

366 scenarios, leads to an increase of the mean value of Q_c. This is so because the dispersion of the

367 intruding saltwater wedge is diminished and the travel time of solutes to the well tends to increase.

368 High values of the natural head gradient of the incoming freshwater, *J*, are associated with high mean

369 values of Q_c. This is consistent with the observation that the inland penetration of the wedge is

370 contrasted by the effect of freshwater which flows in the opposite direction. As expected, decreasing

371   x_w (moving the pumping well towards the coast) leads to a reduction of the mean value of Q_c. Figure

372   4a shows that mean Q_c varies with x_w and J in a similar way. This outcome is consistent with Eq.

373   (27) where Q_c depends on the product $x_w J$, i.e., increasing x_w or J has the same effect on Q_c.

374   It can be noted (see Tab. 3) that $AMAE_{Pe_T}$ is smaller than $AMAE_J$ and $AMAE_{x_w}$, consistent

375   with Fig. 4a. Figure 4b shows that the variance of Q_c decreases as Pe_T, J, or x_w increase. This trend

376   suggests that the uncertainty on Q_c, as quantified by the variance, decreases as (*i*) the intruding wedge

377   sharpens or is pushed toward the seaside boundary by the incoming freshwater or (*ii*) the well is

378   placed at increasing distance from the coastline. Inspection of Fig. 4c and 4d shows that conditioning

379   on Pe_T, J, or x_w causes the *pdf* of Q_c to become less asymmetric and less tailed than its unconditional

380   counterpart. This behavior suggests that the relative frequency of occurrence of (high or low) extreme

381   values of Q_c tends to decrease as additional information about the model parameters become

382   available.

383   Figure 5 depicts error, e_j, Eq. (26) versus total degree, *w*, of the gPCE representation of Q_c,

384   for *j* = (a) $AMAE_{x_i}$, (b) $AMAV_{x_i}$, (c) $AMA\gamma_{x_i}$ and (d) $AMAk_{x_i}$ ($x_i = Pe_T$ (blue curves), J (red

385   curves), x_w (green curves)). These results indicate that: (*i*) e_j associated with $AMAE_{x_i}$ is negligible

386   ($\approx 1\%$) even for low *w*; (*ii*) $e_{AMAV_{Pe_T}} \approx 10\%$ for *w* = 2 and rapidly decreases to values below 1% for

387   increasing *w*; (*iii*) e_{AMAV_J} and $e_{AMAV_{x_w}}$ are always smaller than 1%; and (*iv*) the trend of $e_{AMA\gamma_{x_i}}$ is

388   similar to that of $e_{AMAk_{x_i}}$ for all x_i, with values of the order of 10% or higher for *w* = 2 and displaying

389   a decrease with increasing *w* to then stabilize around values smaller than 1% when $w \approx 4$ or 5. We

390   note that the absolute relative error (26) for $AMAE_{x_i}$ with a given value of *w* is always lower than

391   errors associated with higher order moments. Similar to our results in Section 3.1, it is clear from Fig.

392   5 that attaining a given level of accuracy for the gPCE based indices for Q_c requires considering a

393 diverse total order w of the gPCE depending on the order of the statistical moment considered. As

394 such, following the typical practice of assessing the reliability of a gPCE surrogate model solely on

395 the basis of the variance or of a few random model realizations does not guarantee a satisfactory

396 accuracy of the uncertainty analysis of a target model output which should consider higher-order

397 statistical moments.

3.3 Solute transport in a laboratory-scale porous medium with zoned heterogeneity

399   As a last exemplary showcase, we consider the laboratory-scale experimental analysis of

400 nonreactive chemical transport illustrated by Esfandiar et al. (2015). These authors consider tracer

401 transport within a rectangular flow cell filled with two types of uniform sands. These were

402 characterized by diverse porosity and permeability values, which were measured through separate,

403 standard laboratory tests. A sketch of the experimental set-up displaying the geometry of the two

404 uniform zones respectively formed by coarse and fine sand is illustrated in Fig. 6.

405   After establishing fully saturated steady-state flow, a solution containing a constant tracer

406 concentration is injected as a step input at the cell inlet. The tracer breakthrough curve is then defined

407 in terms of the temporal variation of the spatial mean of the concentration detected along the flow

408 cell outlet. Esfandiar et al. (2015) modeled the temporal evolution of normalized (with respect to the

409 solute concentration of the injected fluid) concentration at the outlet, $\overline{C}(t)$ (t denoting time), by

410 numerically solving within the flow domain the classical Advection-Dispersion Equation

411 implementing an original and accurate space-time grid adaptation technique. Unknown longitudinal

412 dispersivities of the two sands ($a_{L,i}$, $i = 1, 2$ respectively denoting the coarse and fine sand) were

413 considered as uncertain system parameters to be estimated against the available experimental solute

414 breakthrough data. To minimize the computational costs in the model calibration process, Esfandiar

415 et al. (2015) relied on a gPCE approximation of $\overline{C}(t)$. The authors constructed a gPCE of total degree

416 $w = 3$ by considering $\log_{10}\left(a_{L,i}\right)$ to be two *i.i.d.* random variables uniformly distributed within

417     $\Gamma_{\log_{10}(a_{L,i})} = [-6, -2]$, $a_{L,i}$ being expressed in [m]. Further details about the problem set-up, numerical

418   discretization and grid adaptation technique as well of the construction of the gPCE representation

419   can be found in Esfandiar et al. (2015). Here, we ground the application of our new GSA metrics on

420   the gPCE surrogate model already constructed by Esfandiar et al. (2015) to approximate $\overline{C}(t)$.

421   Figure 7 depicts the temporal evolution of the unconditional expected value, $E\left[\overline{C}(t)\right]$,

422   variance, $V\left[\overline{C}(t)\right]$, skewness, $\gamma\left[\overline{C}(t)\right]$, and kurtosis, $k\left[\overline{C}(t)\right]$, of normalized $\overline{C}(t)$. Time steps

423     $t_{0.02}$, $t_{0.4}$, and $t_{0.96}$, i.e., the times at which $E\left[\overline{C}(t)\right]$ = 0.02, 0.4, and 0.96, respectively, are

424   highlighted in Fig. 7a. Figure 7a reveals a pronounced tailing of $E\left[\overline{C}(t)\right]$ at late times, the short

425   time mean breakthrough being associated with a rapid temporal increase of $E\left[\overline{C}(t)\right]$. A local

426   minimum at $t_{0.4}$ and two local peaks and are recognized in $V\left[\overline{C}(t)\right]$ (Fig. 7b). The variance peaks

427   at times approximately corresponding to the largest values of $\partial^2 E\left[\overline{C}(t)\right]/\partial t^2$. This outcome is

428   consistent with the results of numerical Monte Carlo (MC) simulations depicted in Fig. 8 of Esfandiar

429   et al. (2015) where the largest spread of the MC results is observed around these locations. The local

430   minimum displayed by $V\left[\overline{C}(t)\right]$ suggests that $\overline{C}(t)$ at observation times close to $t_{0.4}$ is mainly

431   driven by advection, consistent with the observation that advective transport components are the main

432   driver of the displacement of the center of mass of a solute plume. The late time variance $V\left[\overline{C}(t)\right]$

433   tends to vanish because the normalized breakthrough curve is always very close to unity irrespective

434   of the values of $a_{L,1}$ and $a_{L,2}$. Joint inspection of Fig.s 7c and 7d reveals that the *pdf* of $\overline{C}(t)$ tends to

435   be symmetric around the mean (Fig. 7c) and characterized by light tails (Fig. 7d) at about $t_{0.4}$.

436   Otherwise, the *pdf*s of $\overline{C}(t)$ tends to display heavy right or left tails, respectively for observation

437   times shorter or longer than $t_{0.4}$. These observations suggest that the relative frequency of rare events

438   (i.e., very low or high solute concentrations, which can be of some concern in the context of risk

439   assessment) is lowest at intermediate observation times across the duration of the experiment.

440   Figure 8 depicts the temporal evolution of (*a*) $AMAE_{x_i}$, (*b*) $AMAV_{x_i}$, (*c*) $AMA\gamma_{x_i}$, and (*d*)

441    $AMAk_{x_i}$ ($x_i = \log_{10}(a_{L,1})$, $\log_{10}(a_{L,2})$) of $\overline{C}(t)$. Results embedded in Fig. 8 show that statistical

442   moments of $\overline{C}(t)$ are more sensitive to $\log_{10}(a_{L,1})$ than to $\log_{10}(a_{L,2})$ at early times. The opposite

443   occurs when $t > t_{0.4}$. Our set of results suggests that the overall early time pattern of solute

444   breakthrough is mainly dictated by the value of $a_{L,1}$, the late time behavior being chiefly influenced

445   by $a_{L,2}$. These conclusions are supported by the results of Fig.s 9-11, where we depict the expected

446   value, variance, skewness, and kurtosis of $\overline{C}(t)$ conditional to $\log_{10}(a_{L,1})$ (blue curves) and

447    $\log_{10}(a_{L,2})$ (red curves), at times $t = t_{0.02}$ (Fig. 9), $t_{0.4}$ (Fig. 10), and $t_{0.96}$ (Fig. 11). The corresponding

448   unconditional moments are also depicted (black curves) for ease of comparison. Figure 9 shows that

449   the first four statistical moments of $\overline{C}(t_{0.02})$ are practically insensitive to the value of the fine sand

450   dispersivity, $a_{L,2}$. As one could expect by considering the relative size and geometrical pattern of the

451   two sand zones, Fig. 9a shows that the average amount of solute reaching the cell outlet at early times

452   increases with $a_{L,1}$, because dispersion of solute increases through the coarse sand which resides in

453   the largest portion of the domain. Figure 9b shows $V\left[\overline{C}(t_{0.02})\right]$ is negligible when $a_{L,1}$ is known.

454   Consistent with this result, Fig.s 9c and 9d respectively show a reduction in the asymmetry and in the

455   tailing behavior of the *pdf* of $\overline{C}(t_{0.02})$ when $a_{L,1}$ is fixed. These results are a symptom of a reduced

456   process uncertainty, which is in line with the observation that the bulk of the domain is filled with the

457   coarse sand whose dispersive properties become deterministic when $a_{L,1}$ is known.

458   Inspection of the first four unconditional statistical moments of $\overline{C}(t_{0.4})$ (black curves in Fig.

459   10) indicates that the unconditional *pdf* of $\overline{C}$ at this intermediate time is closely resembling a

460   Gaussian distribution. Conditioning $\overline{C}(t_{0.4})$ on dispersivity causes a variance reduction, an increase

461   of the tailing and the appearance of a negative (left) or positive (right) skewness, respectively when

462   conditioning is performed on $a_{L,1}$ or $a_{L,2}$. The latter behavior suggests that in the type of experimental

463   setting analyzed the variability of $a_{L,1}$ promotes the appearance of values of $\overline{C}(t_{0.4})$ larger than the

464   mean, the opposite occurring when solely $a_{L,2}$ is considered as uncertain.

465   Figure 11 shows that all four statistical moment of $\overline{C}(t_{0.96})$ are chiefly sensitive to the

466   dispersivity of the fine sand box, which is placed near the cell outlet. One can note that knowledge of

467     $a_{L,2}$ yields a diminished variance of $\overline{C}(t_{0.96})$, which drops almost to zero, an increased degree of

468   symmetry and a reduce tailing of the *pdf* of $\overline{C}(t_{0.96})$, all these evidences being symptoms of

469   uncertainty reduction.

470   Results depicted in Fig.s 9-11 and our earlier observations about Fig. 7 are consistent with the

471   expected behavior of transport in the system and the relative role of the dispersivities of the two sand

472   regions. The high level of sensitivity of $\overline{C}(t)$ to $a_{L,1}$ at the early times of solute breakthrough is in

473   line with the observation that solute particles are mainly advected and dispersed through the coarse

474   sand. Both dispersivities affect the behavior of $\overline{C}(t)$ at intermediate times, when solute is traveling

475   through both sands. The dispersivity of the coarse sand plays a minor role at late times, because

476   virtually no concentration gradients arise in this portion of the domain. Otherwise, concentration

477   gradients persist in the fine sand zone close to the outlet and the solute breakthrough is clearly

478   controlled by the dispersive properties of the fine sand.

479   **4. Conclusions**

480   We introduce a set of new indices to be employed in the context of global sensitivity analysis,

481   GSA, of hydrological and Earth systems. These indices consider the first four (statistical) moments

482   of the probability density function, *pdf,* of a desired model output, *y*. As such, they quantify the

expected relative variation, due to the variability in one (or more) model input parameter(s) of the expected value, variance, skewness and kurtosis of y. When viewed in the current research trend, our work is intended to bridge the gap between variance-based and *pdf*-based GSA approaches since it embeds the simplicity of the former while allowing for a higher-order description of how the structure of the *pdf* of y is affected by variations of uncertain model parameters. We cope with computational costs, which might be high when evaluating higher-order moments, by coupling our GSA approach with techniques approximating the full model response through a surrogate model. For the sake of our study, we consider the generalized Polynomial Chaos Expansion (gPCE), other model reduction techniques being fully compatible with our approach. Our new indices can be of interest in applications in the context of current practices and evolution trends in factor fixing procedures (i.e., assessment of the possibility of fixing a parameter value on the basis of the associated output sensitivity), design of experiment, uncertainty quantification and environmental risk assessment, due to the role of the key features of a model output *pdf* in such analyses.

We test and exemplify our methodology on three testbeds: (*a*) the Ishigami function, which is widely employed to test sensitivity analysis techniques, (*b*) the evaluation of the critical pumping rate to avoid salinization of a pumping well in a coastal aquifer, and (*c*) a laboratory-scale nonreactive transport experiment. Our theoretical analyses and application examples lead to the following major conclusions.

1. The ==calculated== sensitivity of a model output, y, with respect to a parameter depends on the selected global sensitivity index, i.e., variability of a model parameter affects statistical moments of y in different ways and with different relative importance, depending on the statistical moment considered. Relying on the indices we propose allows enhancing our ability to quantify how model parameters affect features of the model output *pdf*, such as mean, degree of spread, symmetry and tailedness, in a straightforward and easily transferrable way.

2. Joint inspection of our moment-based global sensitivity indices and of the first four statistical conditional and unconditional moments of y increases our ability to understand the way the

509   structure of the model output *pdf* is controlled by model parameters. As demonstrated in our

510   examples, classical variance-based GSA methods cannot be used for this purpose, leading, in

511   some cases, to the unwarranted conclusion that a given parameter have a limited impact on a

512   target output.

513   3. Analysis of the errors associated with the use of a surrogate model for the evaluation of our

514   moment-based sensitivity indices suggests that: (*a*) attaining a given level of accuracy for the

515   gPCE based indices associated with a target variable, *y*, might require considering a diverse total

516   order *w* of the gPCE, depending on the target statistical moment considered in the GSA of *y*; and

517   (*b*) in our examples, the absolute relative error (26) for $AMAE_{x_i}$ based on a given total degree *w*

518   of the gPCE approximation is always lower than its counterpart associated with higher order

519   moments (see Fig. 2 and 5).

520

521

References

Borgonovo, E.: A new uncertainty importance measure, Reliability Eng. Syst. Safety, 92, 771-784, 2007.

Borgonovo, E., Castaings, W., and Tarantola, S.: Moment Independent Importance Measures: New Results and Analytical Test Cases, Risk Anal., 31, 404-428, 2011.

Chu, J., Zhang, C., Fu, G., Li, Y. and Zhou, H.: Improving multi-objective reservoir operation optimization with sensitivity-informed dimension reduction, Hydrol. Earth Syst. Sci., 19, 3557-3570, doi:10.5194/hess-19-3557-2015, 2015.

Chun, M. H., Han, S. J. and Tak, N. I. L.: An uncertainty importance measure using a distance metric for the change in a cumulative distribution function, Reliab. Eng. Syst. Saf., 70, 313-321, 2000.

Ciriello, V., Di Federico, V., Riva, M., Cadini, F., De Sanctis, J., Zio, E. and Guadagnini, A.: Polynomial chaos expansion for global sensitivity analysis applied to a model of radionuclide migration in a randomly heterogeneous aquifer, Stoch. Environ. Res. Risk. Assess., 27, 945-954, doi: 10.1007/s00477-012-0616-7, 2013.

Colombo, I., Porta, G.M., Ruffo, P. and Guadagnini, A.: Uncertainty quantification of overpressure buildup through inverse modeling of compaction processes in sedimentary basins, Hydrogeol. J., doi:10.1007/s10040-016-1493-9, 2016.

Crestaux, T., Le Maître, O. and Martinez, J. M.: Polynomial chaos expansion for sensitivity analysis, Reliab. Eng. Syst. Safety, 94(7), 1161-1172, doi: org/10.1016/j.ress.2008.10.008, 2009.

Elshorbagy, A., Corzo, G., Srinivasulu, S., and Solomatine, D. P.: Experimental investigation of the predictive capabilities of data driven modeling techniques in hydrology - Part 1: Concepts and methodology, Hydrol. Earth Syst. Sci., 14, 1931-1941, doi:10.5194/hess-14-1-2010, 2010a.

Elshorbagy, A., Corzo, G., Srinivasulu, S. and Solomatine, D. P.: Experimental investigation of the predictive capabilities of data driven modeling techniques in hydrology - Part 2: Application, Hydrol. Earth Syst. Sci., 14, 1943-1961, doi:10.5194/hess-14-1943-2010, 2010b.

Esfandiar, B., Porta, G., Perotto, S. and Guadagnini, A.: Impact of space-time mesh adaptation on solute transport modeling in porous media, Water Resour. Res., 51, 1315-1332, doi:10.1002/2014WR016569, 2015.

Formaggia, L., Guadagnini, A., Imperiali, I., Lever, V., Porta, G., Riva, M., Scotti, A. and Tamellini, L.: Global sensitivity analysis through polynomial chaos expansion of a basin-scale geochemical compaction model, Comput. Geosci., 17, 25-42, doi:org/10.1007/s10596-012-9311-5, 2013.

Förster, K., Meon, G., Marke, T. and Strasser, U.: Effect of meteorological forcing and snow model complexity on hydrological simulations in the Sieber catchment (Harz Mountains, Germany), Hydrol. Earth Syst. Sci., 18, 4703-4720, doi:10.5194/hess-18-4703-2014, 2014.

Fu, G., Kapelan, Z. and Reed, P.: Reducing the complexity of multiobjective water distribution system optimization through global sensitivity analysis, J. Water Resour. Plann. Manage., 38(3), 196-207, doi:0.1061/(ASCE)WR.1943-5452.0000171, 2012.

Ghanem, R. G and Spanos, P. D.: Stochastic finite elements: a spectral approach, Berlin: Springer; 1991.

Gläser, D., Dell'Oca, A., Tatomir, A., Bensabat, J., Class, H., Guadagnini, A., Helmig, R., McDermott, C., Riva, M., and Sauter, M.: An approach towards a FEP-based model risk assessment for hydraulic fracturing operations, Energ. Procedia, 97, 387-394, 2016.

Grauso, G., Fattoruso, G., Crocetti C. and Montanari, A.: A spatially distributed analysis of erosion susceptibility and sediment yield in a river basin by means of geomorphic parameters and regression relationships, Hydrol. Earth Syst. Sci. Discussions, 4, 627-654, 2007.

Hartmann, A., Weiler, M., Wagener, T., Lange, J., Kralik, M., Humer, F., Mizyed, N., Rimmer, A., Barbera, J. A., Andreo, B., Butscher, C. and Huggenberger, P.: Process-based karst modelling to relate hydrodynamic and hydrochemical characteristics to system properties, Hydrol. Earth Syst. Sci., 17, 3305-3321, doi:10.5194/hess-17-3305-2013, 2013.

Herman, J. D., Kollat, J. B., Reed, P. M. and Wagener, T.: From maps to movies: high-resolution time-varying sensitivity analysis for spatially distributed watershed models, Hydrol. Earth Syst. Sci., 17, 5109-5125, doi:10.5194/hess-17-5109-2013, 2013.

Homma, T. and Saltelli, A.: Importance measures in global sensitivity analysis of nonlinear models, Reliab. Eng. Syst. Saf., 52, 1-17, 1996.

Iman, R.L. and Hora, S. C.: A robust measure of uncertainty importance for use in fault tree system analysis, Risk Anal., 10(3), 401-406, 1990.

Koutsoyiannis, D.: "A random walk on water", Hydrol. Earth Syst. Sci., 14, 585-601, 2010.

Krykacz-Hausmann, B.: Epistemic sensitivity analysis based on the concept of entropy, In: Prado, P., Bolado, R. (Eds.), Proceedings of SAMO2001, Madrid, pp. 31-35, 2001.

Le Maître, O. P. and Knio, O. M.: Spectral methods for uncertainty quantification, Scientific computation, Springer, 2010.

Paniconi, C. and Putti, M.: Physically based modeling in catchment hydrology at 50: survey and outlook, Water Resour. Res., 51, 7090-7129, doi:10.1002/ 2015WR017780, 2015.

Pianosi, F. and Wagener, T.: A simple and efficient method for global sensitivity analysis based on cumulative distribution functions, Environ. Model. Softw., 67, 1-11, doi: 10.1016/j.envsoft.2015.01.004, 2015.

Pianosi, F., Wagener, T., Beven, K., Freer, J., Hall, J.W., Rougier, J. and Stephenson, D.B.: Sensitivity Analysis of Environmental Models: a Systematic Review with Practical Workflow, Environmental Modelling & Software, 79, 214-232, doi: 10.1016/j.envsoft.2016.02.008, 2016.

Pool, M. and Carrera, J.: A correction factor to account for mixing in Ghyben-Herzberg and critical pumping rate approximations of seawater intrusion in coastal aquifers, Water Resour. Res., 47, W05506, doi:10.1029/2010WR010256, 2011.

Punzo, V., Marcello, M. and Biagio, C.: Do we really need to calibrate all the parameters? Variance-based sensitivity analysis to simplify microscopic traffic flow models, Intel. Trans. Sys. IEEE Trans., 16(1), 184-193, 2015.

Razavi, S. and Gupta H. V.: What do we mean by sensitivity analysis? The need for comprehensive characterization of "global" sensitivity in Earth and Environmental systems models, Water Resour. Res., 51, doi:10.1002/2014WR016527, 2015.

Razavi, S., Tolson, B.A. and Burn, D.H.: Numerical assessment of metamodelling strategies in computationally intensive optimization, Environ. Model. Softw., 34(0), 67-86, doi: 10.1016/j.envsoft.2011.09.010, 2012a.

Razavi, S., Tolson, B.A. and Burn, D.H.: Review of surrogate modeling in water resources. Water Resour. Res. 48 (7), W07401, doi: 10.1029/ 2011WR011527, 2012b.

Riva, M., Guadagnini, A. and Dell'Oca, A.: Probabilistic assessment of seawater intrusion under multiple sources of uncertainty, Adv. Water Resour., 75, 93-104, doi: 10.1016/j.advwatres.2014.11.002, 2015.

Saltelli, A., Ratto, M., Andres, T., Campolongo, F., Cariboni, J., Gatelli, D., Saisana, M., Tarantola, S.: Global Sensitivity Analysis. The Primer. Wiley, 2008.

Sarrazin, F., Pianosi, F. and Wagener, T.: Global sensitivity analysis of enviromental models: convergence and validation, Environ. Model. Softw., 79, 135-152, doi: 10.1016/j.envsoft.2016.02.005, 2016.

Sobol, I. M.: Sensitivity estimates for nonlinear mathematical models, Math. Model. Comput. Exp., 1, 407-417, 1993.

Sudret, B.: Global sensitivity analysis using polynomial chaos expansions, Reliab. Eng. & Syst. Safety, 93, 964-979, doi:10.1016/j.ress.2007.04.002, 2008.

Wagener, T. and Montanari, A.: Convergence of approaches toward reducing uncertainty in predictions in ungauged basins, Water Resour. Res., 47, W060301, doi:10.1029/2010WR009469, 2011.

Wagener, T., Sivapalan, M., Troch, P. A., McGlynn, B. L., Harman, C. J., Gupta, H. V., Kumar, P., Rao, P. S. C., Basu, N. B., and Wilson, J. S.: The future of hydrology: An evolving science for a changing world, Water Resour. Res., 46, W05301, doi:10.1029/2009WR008906, 2010.

Willmann, M., Sanchez-Vila, X., Carrera, J. and Guadagnini, A.: Block-upscaling of transport in heterogeneous aquifers, Calibration and Reliability in Groundwater Modelling: From Uncertainty to Decision Making, Proceedings of ModelCARE 2005, The Hague, The Netherlands, June 2005, IAHS Publ. 304, 2006.

Xiu, D. and Karniadakis, G. E. M.: The Wiener-Askey polynomial chaos for stochastic differential equations, SIAM J. Sci. Comput., 24(2), 619-644, doi: 10.1137/S1064827501387826, 2002.

630

631 **Table 1.** Global sensitivity index $AMAE_{x_i}$ Eq. (10), $AMAV_{x_i}$ Eq. (12), $AMA\gamma_{x_i}$ Eq. (14), and

632 $AMAk_{x_i}$ Eq. (16) associated with the Ishigami function Eq. (18). Principal Sobol' indices, S_{x_i} Eq.

633 (7), are also listed; $x_i = x_1,\ x_2,\ x_3$.

	$AMAE_{x_i}$	$AMAV_{x_i}$	S_{x_i}	$AMA\gamma_{x_i}$	$AMAk_{x_i}$
x_1	0.75	0.40	0.40	0.45	0.37
x_2	0.64	0.29	0.29	0.00	0.33
x_3	0.00	0.84	0.00	0.00	0.53

634

635

636 **Table 2.** Intervals of variations of Pe_T, J, x_w.

	$\Gamma_n = [x_{n,\min} - x_{n,\max}]$
Γ_{Pe_T}	$[0.01 - 0.1]$
Γ_J	$[8e^{-4} - 2.5e^{-3}]$
Γ_{x_w}	$[10 - 33]$

637

638

639 **Table 3.** Global sensitivity index $AMAE_{x_i}$ Eq. (10), $AMAV_{x_i}$ Eq. (12), $AMA\gamma_{x_i}$ Eq. (14), and

640 $AMAk_{x_i}$ Eq. (16) associated with the critical pumping rate Q_c (25). Principal Sobol' indices, S_{x_i} Eq.

641 (7), are also listed; $x_i = Pe_T$, J, x_w.

	$AMAE_{x_i}$	$AMAV_{x_i}$	S_{x_i}	$AMA\gamma_{x_i}$	$AMAk_{x_i}$
Pe_T	0.07	0.14	0.09	0.35	0.09
J	0.14	0.41	0.41	0.88	0.12
x_w	0.15	0.48	0.48	0.78	0.11

642

643

644
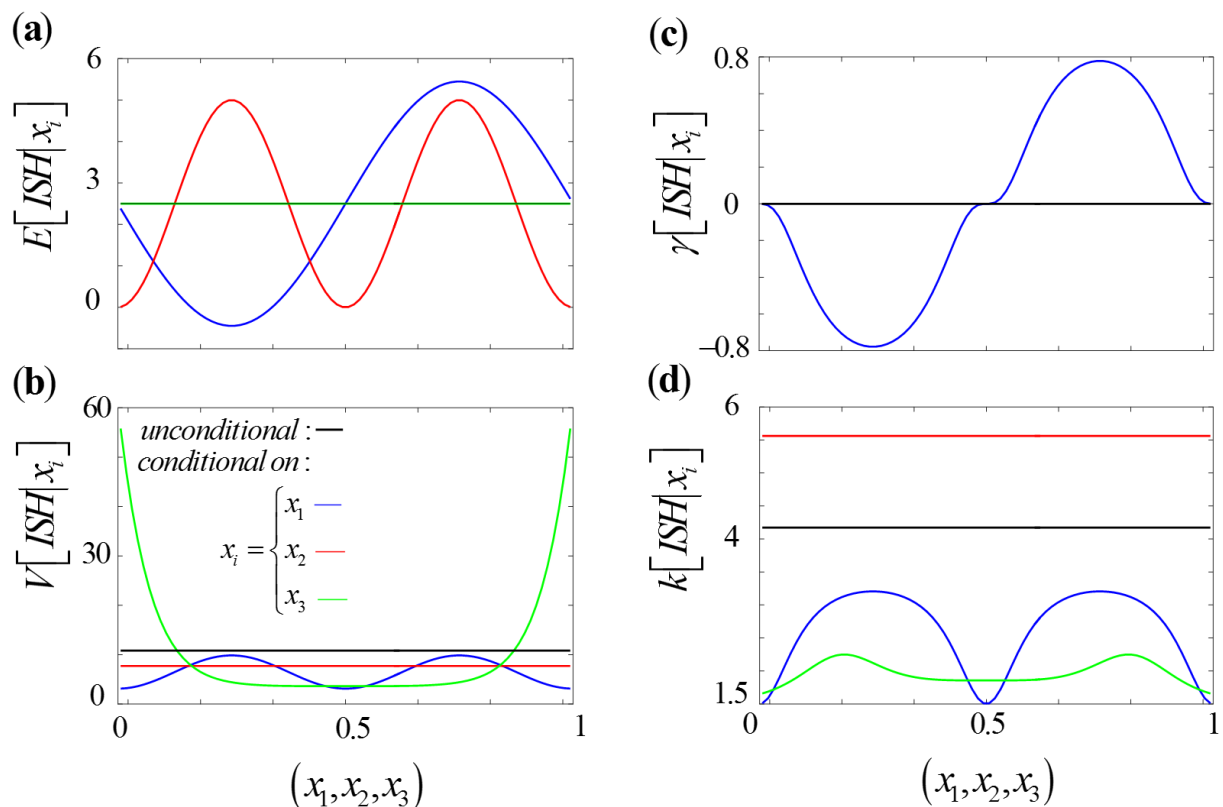
Figure 1. Variation of the first four moments of *ISH* Eq. (18) conditional to values of x_1 (blue curves), x_2 (red curves) and x_3 (green curves) within the parameter space: (**a**) expected value, $E[ISH \mid x_i]$, (**b**) variance, $V[ISH \mid x_i]$, (**c**) skewness, $\gamma[ISH \mid x_i]$, and (**d**) kurtosis, $k[ISH \mid x_i]$, (i = 1, 2, 3). The corresponding unconditional moments (black curves) are also depicted.

649

650
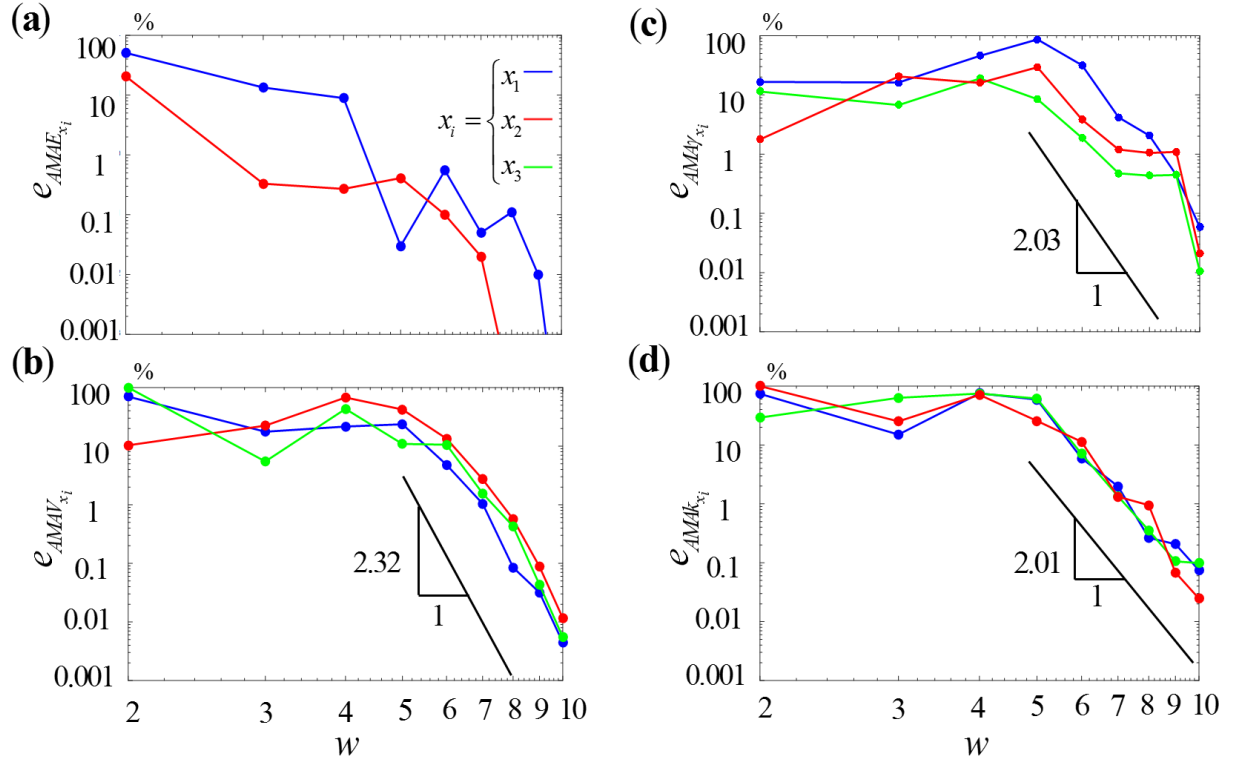
Figure 2. Error e_j Eq. (26) versus the total degree w of the gPCE representation of ISH for $j =$ (**a**) $AMAE_{x_i}$, (**b**) $AMAV_{x_i}$, (**c**) $AMA\gamma_{x_i}$ and (**d**) $AMAk_{x_i}$, with $x_i = x_1$ (blue curves), x_2 (red curves), x_3 (green curves). Note that $AMAE_{x_3}$ is always smaller than 0.001%. Average slope of the rate of decrease of e_j for the largest w values considered are indicated as a reference in (**a**)-(**d**).

655

656

657
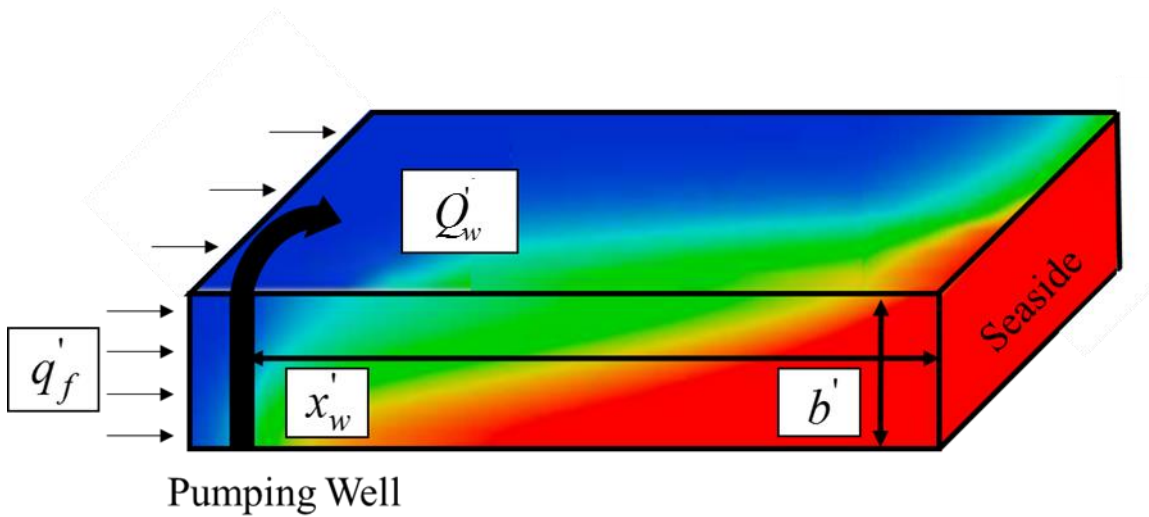
Figure 3. Sketch of the critical pumping scenario taking place within a coastal aquifer of thickness b'. A constant freshwater (in blue) flux, q'_f, flows from the inland to the coastline (saltwater in red). A constant discharge, Q'_w, is pumped from a fully penetrating well located at a distance x'_w from the coastline. Color scale indicating variable concentration of salt is only qualitative for illustration purposes.

663

664
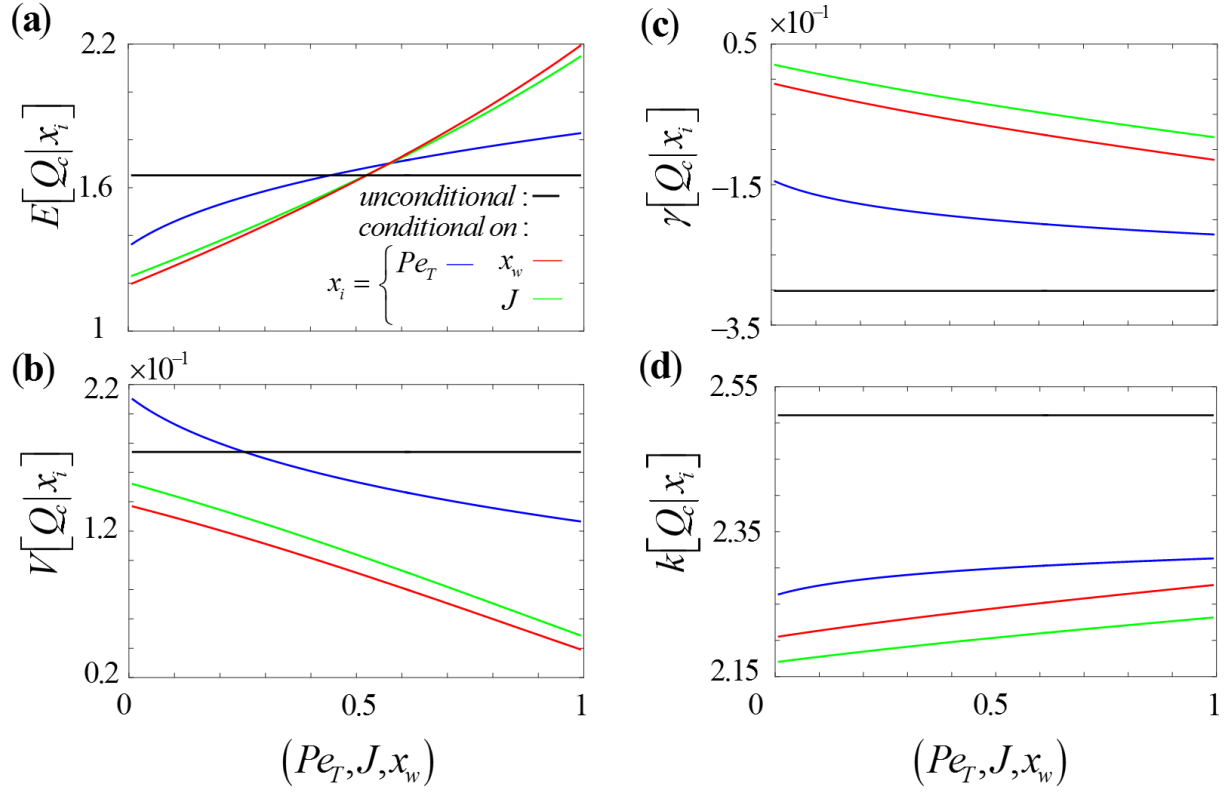
Figure 4. First four moments of Q_c Eq. (27) conditional to values of Pe_T (blue curves), J (green curves), and x_w (red curves) within the parameter space: (**a**) expected value, $E[Q_c \mid x_i]$, (**b**) variance, $V[Q_c \mid x_i]$, (**c**) skewness, $\gamma[Q_c \mid x_i]$, and (**d**) kurtosis, $k[Q_c \mid x_i]$, ($x_i = Pe_T$, J, x_w). The corresponding unconditional moments (black curves) are also depicted. Intervals of variation of Pe_T, J and x_w has been rescaled between zero and one for graphical representation purposes.

670

671

672

673
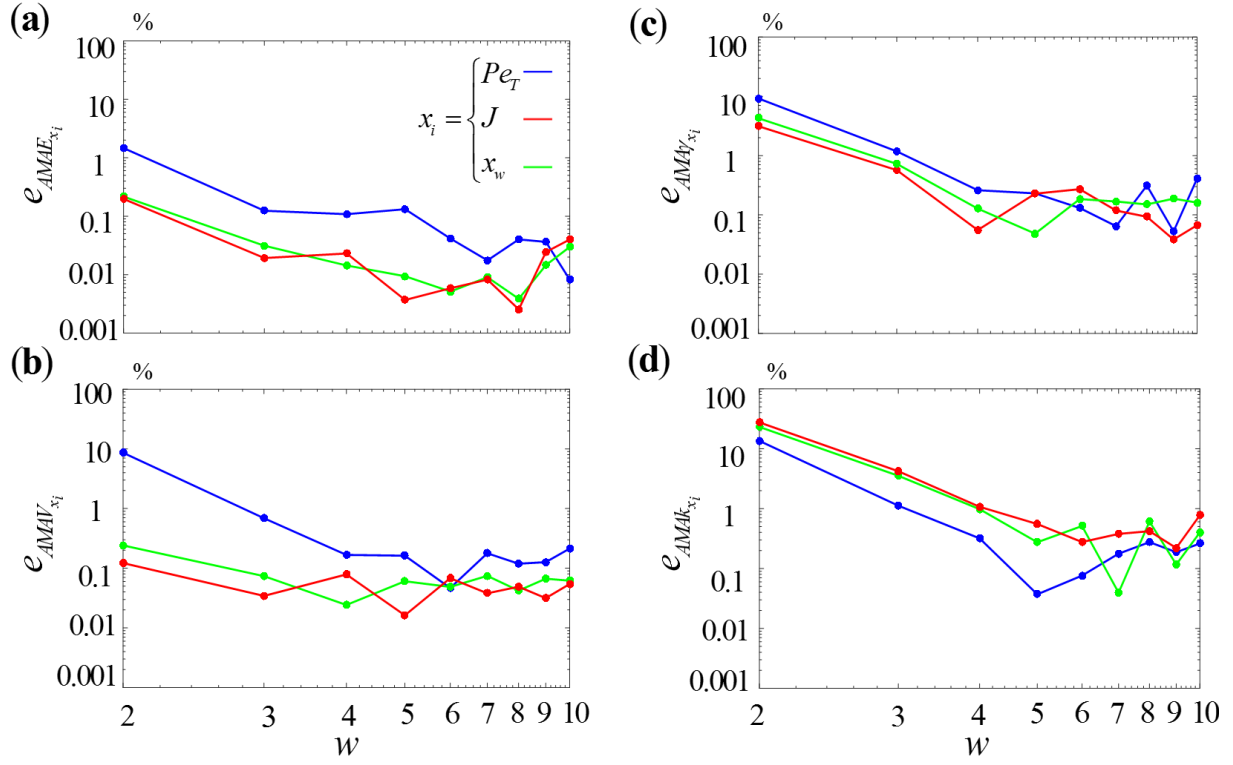
Figure 5. Error e_j Eq. (26) versus total degree w of the gPCE representation of Q_c, for j = (**a**) $AMAE_{x_i}$, (**b**) $AMAV_{x_i}$, (**c**) $AMA\gamma_{x_i}$ and (**d**) $AMAk_{x_i}$, $x_i = Pe_T$ (blue curves), J (red curves), x_w (green curves).
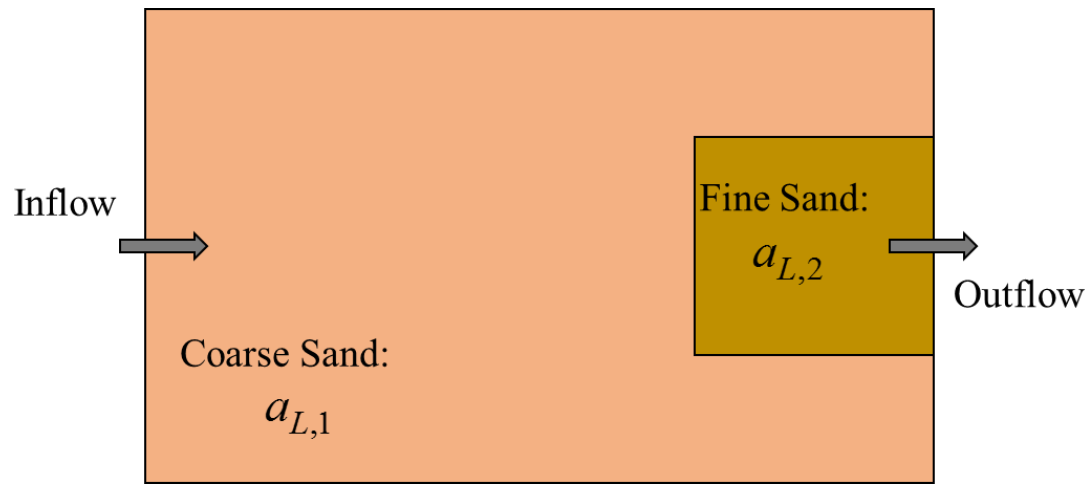
680

681 **Figure 6.** Sketch of the solute transport setting considered by Esfandiar et al. (2015).

682

683

684
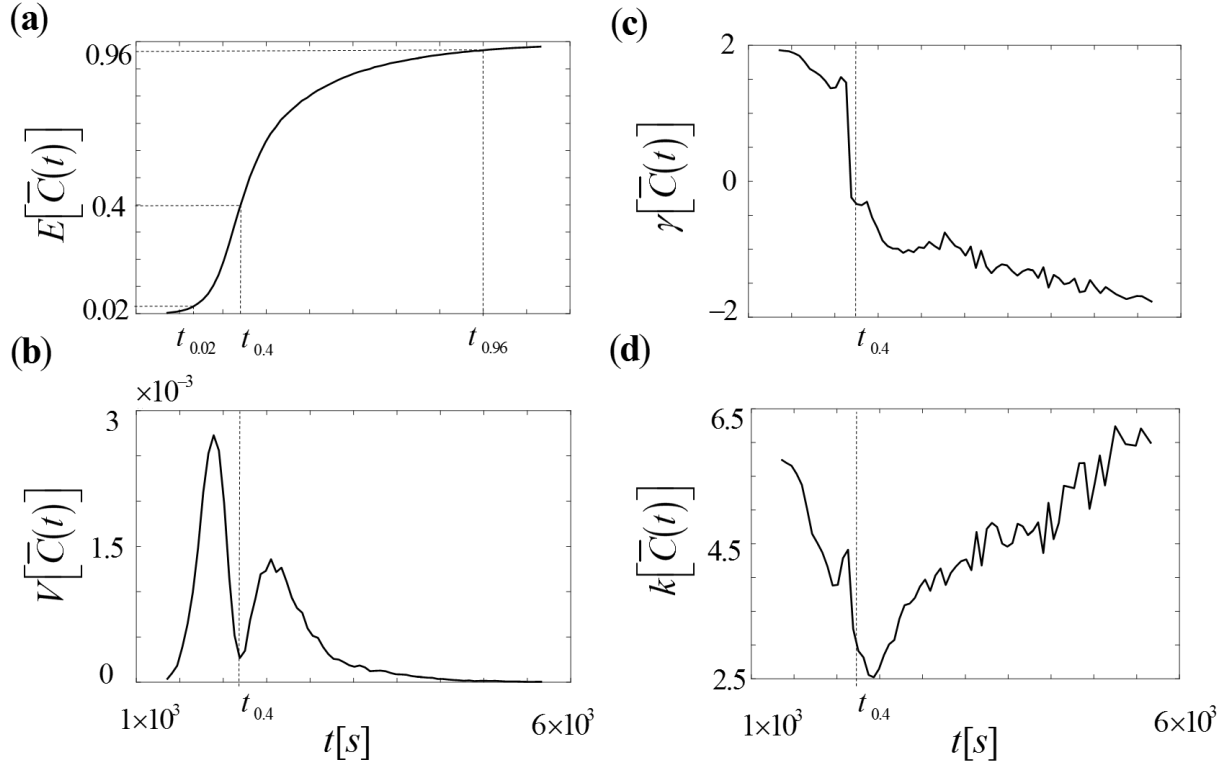
Figure 7. Temporal evolution of the unconditional (*a*) expected value, $E\left[\overline{C}(t)\right]$, (**b**) variance, $V\left[\overline{C}(t)\right]$, (**c**) skewness, $\gamma\left[\overline{C}(t)\right]$, and (**d**) kurtosis, $k\left[\overline{C}(t)\right]$, of normalized $\overline{C}(t)$. Vertical lines in (*a*) correspond to time steps $t_{0.4}$, $t_{0.02}$ and $t_{0.96}$, i.e., the times at which $E\left[\overline{C}(t)\right] = 0.02, 0.4,$ and 0.96, respectively.

689

690

691

692
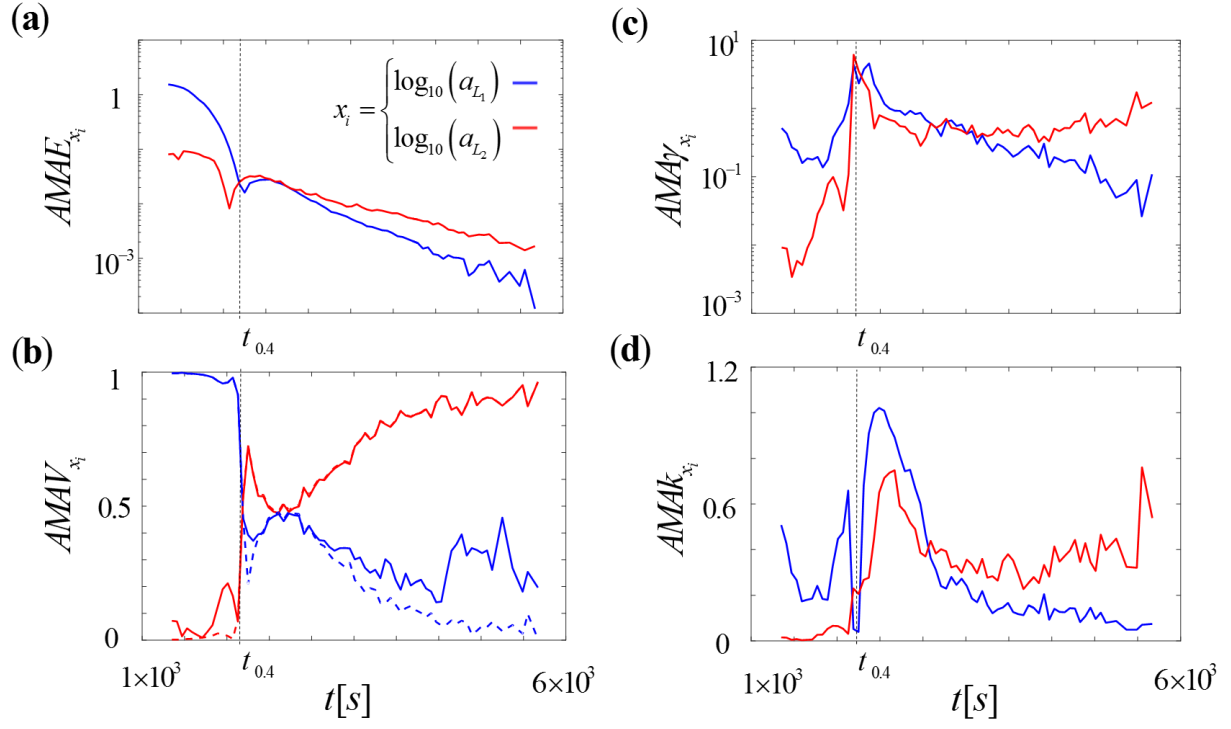
Figure 8. Time evolution of the global sensitivity index (**a**) $AMAE_{x_i}$, (**b**) $AMAV_{x_i}$ and S_{x_i} (dashed curves), (**c**) $AMA\gamma_{x_i}$, and (**d**) $AMAk_{x_i}$ of $\overline{C}(t)$ ($x_i = \log_{10}(a_{L,1})$ (blue), or $\log_{10}(a_{L,2})$ (red)).

697
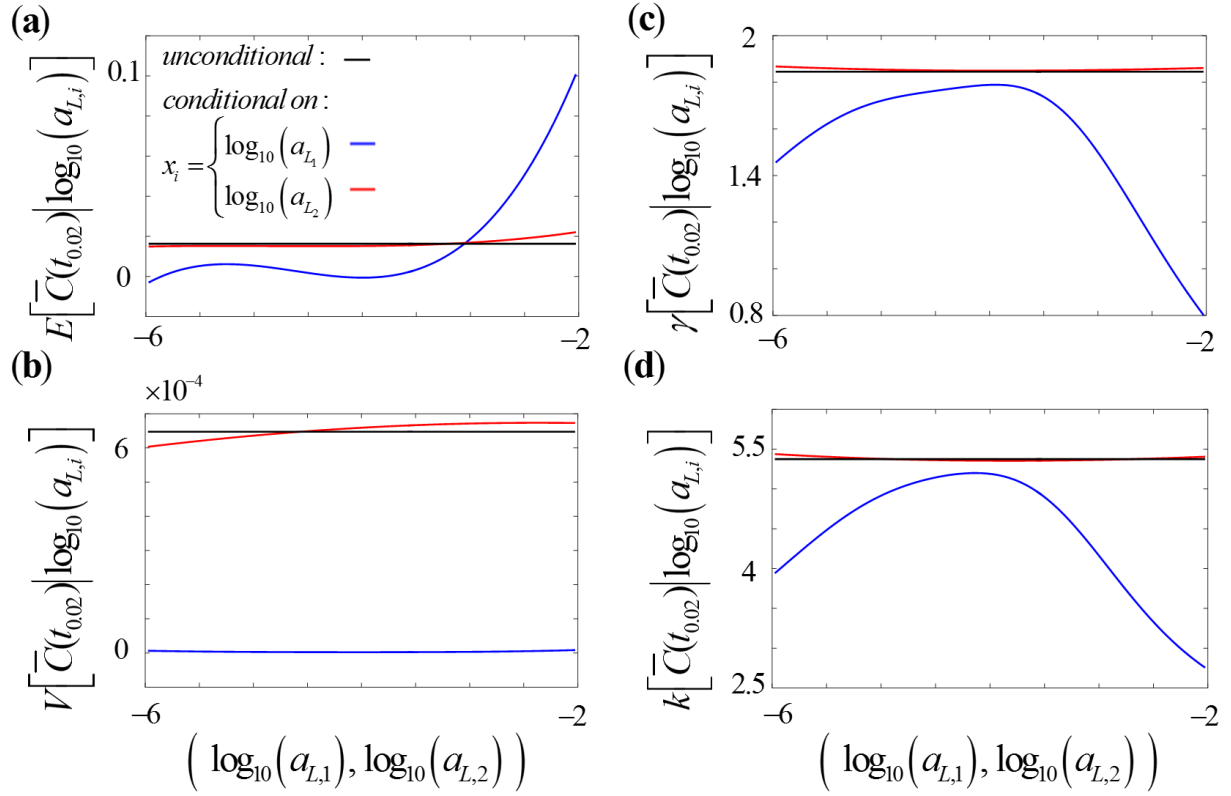
Figure 9. First four moments of $\overline{C}(t = t_{0.02})$ conditional on $\log_{10}(a_{L,1})$ (blue curves) and $\log_{10}(a_{L,2})$ (red curves), at time $t = t_{0.02}$: (**a**) expected value, $E\left[\overline{C}(t_{0.02})\middle|\log_{10}\left(a_{L,i}\right)\right]$, (**b**) variance, $V\left[\overline{C}(t_{0.02})\middle|\log_{10}\left(a_{L,i}\right)\right]$, (**c**) skewness, $\gamma\left[\overline{C}(t_{0.02})\middle|\log_{10}\left(a_{L,i}\right)\right]$, and (**d**) kurtosis, $k\left[\overline{C}(t_{0.02})\middle|\log_{10}\left(a_{L,i}\right)\right]$ ($i = 1, 2$). The corresponding unconditional moments are also depicted (black curves).

707
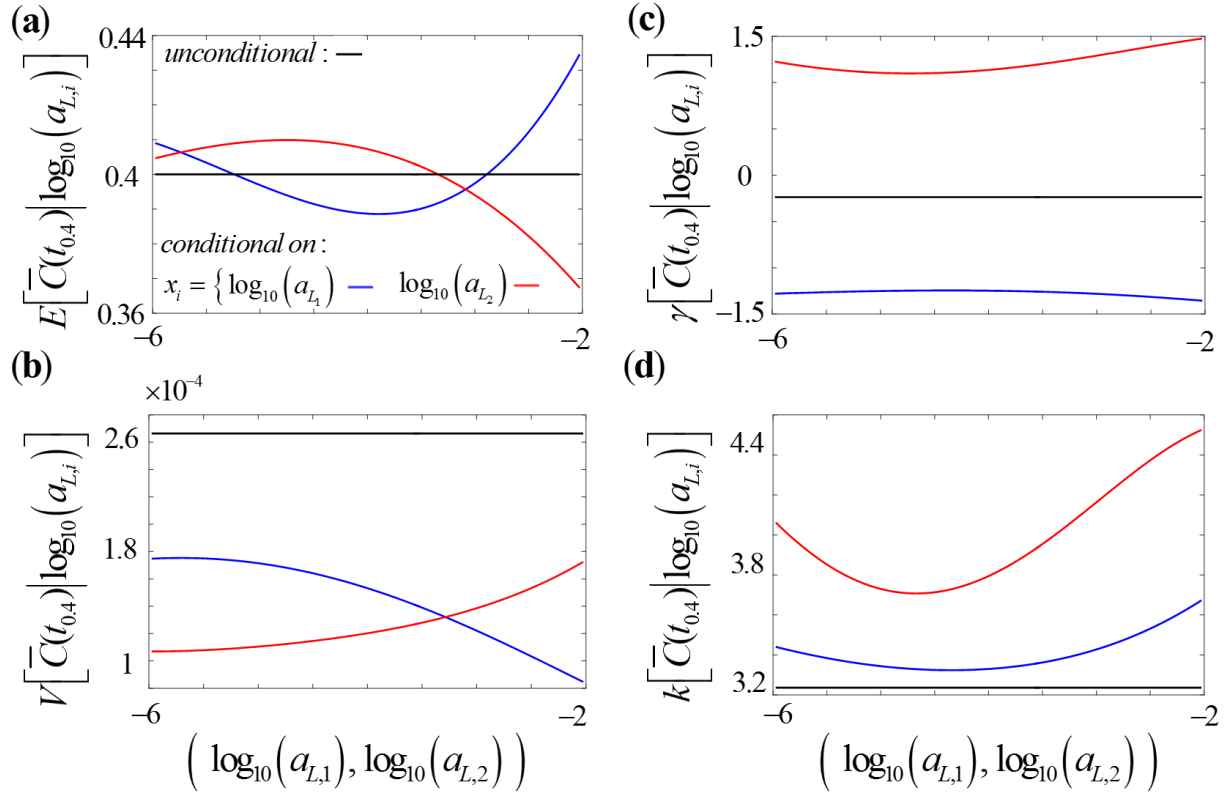
Figure 10. First four moments of $\overline{C}(t = t_{0.4})$ conditional on $\log_{10}(a_{L,1})$ (blue curves) and $\log_{10}(a_{L,2})$ (red curves), at time $t = t_{0.4}$: (**a**) expected value, $E\left[\overline{C}(t_{0.4})\middle|\log_{10}(a_{L,i})\right]$, (**b**) variance, $V\left[\overline{C}(t_{0.4})\middle|\log_{10}(a_{L,i})\right]$, (**c**) skewness, $\gamma\left[\overline{C}(t_{0.4})\middle|\log_{10}(a_{L,i})\right]$, and (**d**) kurtosis, $k\left[\overline{C}(t_{0.4})\middle|\log_{10}(a_{L,i})\right]$ ($i = 1, 2$). The corresponding unconditional moments are also depicted (black curves).

713

714

715
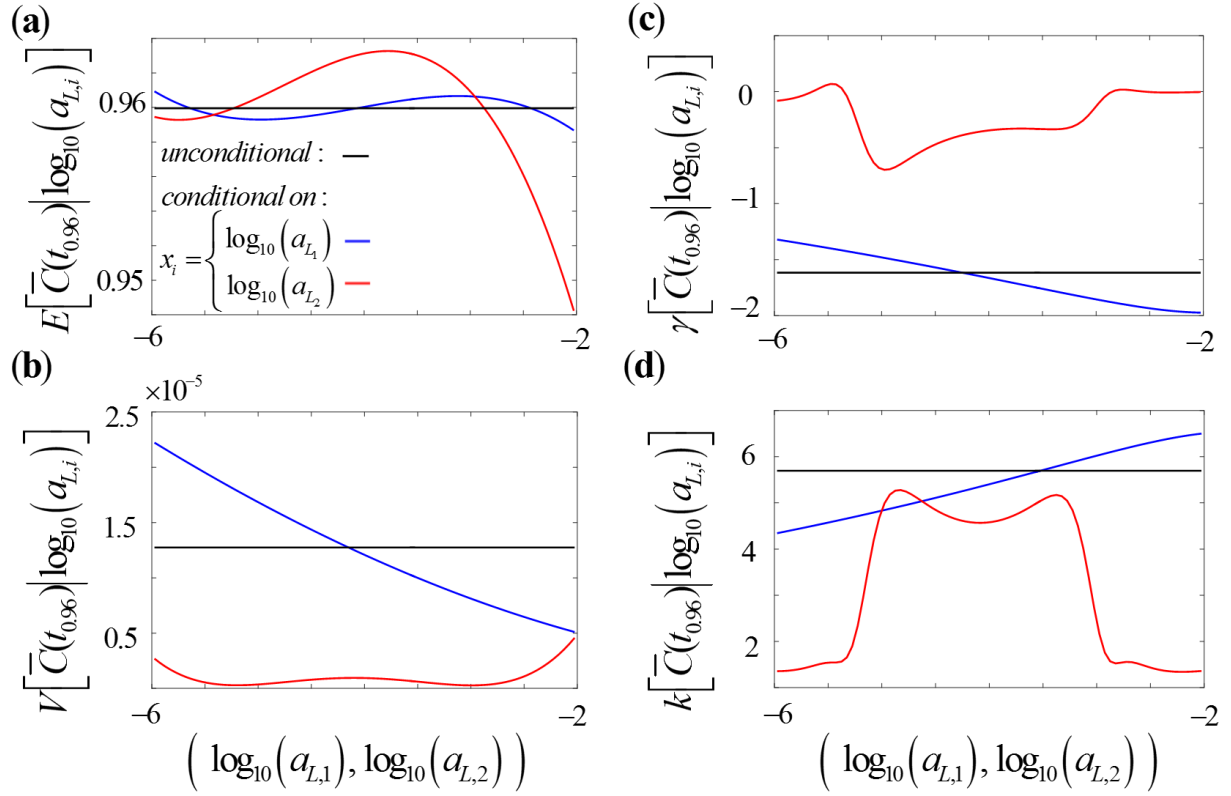
Figure 11. First four moments of $\overline{C}(t = t_{0.96})$ conditional on $\log_{10}(a_{L,1})$ (blue curves) and $\log_{10}(a_{L,2})$ (red curves), at time $t = t_{0.96}$: (**a**) expected value, $E\left[\overline{C}(t_{0.96})\middle|\log_{10}(a_{L,i})\right]$, (**b**) variance, $V\left[\overline{C}(t_{0.96})\middle|\log_{10}(a_{L,i})\right]$, (**c**) skewness, $\gamma\left[\overline{C}(t_{0.96})\middle|\log_{10}(a_{L,i})\right]$, and (**d**) kurtosis, $k\left[\overline{C}(t_{0.96})\middle|\log_{10}(a_{L,i})\right]$ $(i = 1, 2)$. The corresponding unconditional moments are also depicted (black curves).

721